ARC Alliance

ARC Geophysical Research

GR Geophysical Research

Differential Cooling of a Freshwater Body below the Temperature of Maximum Density

Kelsey A. Everard[*1], Edmund Tedford[2], Bernard E. Laval[2], Marc B. Parlange[3], and Gregory A. Lawrence[2]

[1]Courant Institute of Mathematical Sciences, New York University, New York, NY, USA
[2]Civil Engineering, University of British Columbia, Vancouver, Canada
[3]University of Rhode Island, Kingston, RI, USA

Abstract

We propose a simplified model for the time rate of change of average basin temperature for a freshwater lake which has two connected basins: a shallow littoral zone of depth D_1, and a deeper main basin of depth D_2. This system is cooled below the temperature of maximum density (T_{md}) with a constant and uniform outgoing surface heat flux, H_o. The differential cooling that is established via this set-up gives rise to an exchange flow between the two basins which we approximate as a time dependent heat flux controlled by the strength of the time dependent density difference between the two basins.

Our model is a coupled system of two ordinary differential equations which allows for a process based investigation into the importance of exchange on the timing of ice-onset for a lake with a shallow littoral zone. While basin geometry plays a role in the overall timing of ice-onset for the system, it is the relative strength of H_o to the exchange flow related heat flux due to the density anomaly of fresh water, ρ_*, which dictates the behaviour of the cooling system. We show that at sufficiently large values of the heat flux ratio, Φ, the difference in timing of ice onset between the littoral zone and main basin becomes insensitive to the initial conditions in the lake. We use data from Base Mine Lake, Canada, to both verify our model assumptions and evaluate the predictions made by our simple model.

Keywords: Differential Cooling, Temperature of Maximum Density, Exchange Flow

*Corresponding Author
E-mail addresses: kae10022@nyu.edu
doi: https://doi.org/10.5149/ARC-GR.1338

1 Introduction

Littoral zones are the most productive region of a lake, and thus play a vital role to lake ecosystems [e.g., 43]. An important feature of littoral zones is that they cool (and warm) quicker than the deeper pelagic zones in a process called *differential cooling* (or warming). This process is due to depth differences and sets up a baroclinic pressure gradient between the littoral and pelagic zones which ultimately drives an exchange flow between the two regions. This process has been the subject of study for decades, with particular attention given to cooling periods. The circulation pattern set up by differential cooling of a lake is referred to as a *thermal siphon* [e.g., 29]. Thermal siphoning-like circulation is well documented in a number of water bodies around the world, including various regions of the Red Sea [30–32], in 61 near-shore regions of the ocean around the world [19], and in various lakes [7, 12]. In essence, thermal siphons act as transport routes between near-shore zones and deeper interiors. As such, thermal siphons can regulate the thermal environment of littoral water and impact the distribution of organic and inorganic material [e.g., 3, 8, 26], making them important hydrodynamic processes for sensitive near-shore ecosystems like coral reefs [e.g., 28] and for water quality [36].

Given the varied impacts and observations of thermal siphons, researchers have sought to characterise these circulation patterns. Over the past few decades, thermal siphons have been investigated and described using laboratory experiments [e.g., 39, 44, 45], numerical experiments [e.g., 16, 42], and analytical and scaling analyses [e.g., 42]. These studies have explored the role of rotation [e.g., 39], the effects of an unsteady surface forcing [e.g., 22], and the effects of bottom topography [e.g., 38]. However, all of these studies have considered cooling situations where the equation of state can be approximated as linear. In reality, however, many freshwater lakes around the world freeze, necessitating a better understanding of littoral zone cooling both around and below T_{md} and the role of thermal siphon-like circulation on the timing of littoral zone ice onset.

There is a large body of work that focuses on the physics behind one water body above T_{md} and one water body below T_{md} converging, and the associated cabbeling instability [e.g., 15]. Cabbeling occurs around the so-called 'thermal bar', which is the T_{md} isotherm separating the body of water above T_{md} and that below T_{md} [e.g. 9]. While differential cooling is identified as a possible mechanism by which the cabbeling instability can be initiated [e.g. 11], much of the work related to the thermal bar and cabbeling instability are focused on the convergence of lake inflows, like rivers, with the lake itself [e.g. 4]. Furthermore, to our knowledge, no one has considered the effect of a thermal bar on the ice onset time in a lake.

While little has been done in the way of characterising a cooling littoral zone around and below T_{md}, there is a preponderance of work focused on characterising when the surface of a lake might begin to freeze. Simply stated, the surface of a lake should begin to freeze when the water surface temperature is at the appropriate freezing point. Thus, in a broad sense, all models of lake ice onset aim to predict when the water surface temperature reaches this freezing point, which is strongly connected to air temperature [e.g., 23]. Most models to date can be classified as either empirically based ones connecting ice onset with air temperature [e.g., 27, 35] or lake surface heat flux [e.g. 2], or as deterministic 1D hydrodynamic models [e.g. 25]. The problem is that on the one hand, the empirically based models are far too simple, and on the other, the data required to run a 1D hydrodynamic model are typically unavailable. [41] begin to bridge this gap with a more process based approach focused on the combined effect of thermal energy loss due to atmospheric cooling and mechanical energy input from surface wind stresses acting to vertically stir the lake below T_{md}.

All of the models of lake ice onset to our current knowledge assume that the lake in question can be represented in an average sense, that is, lake bathymetry is not included.

This is in large part due to the broadly 1D nature of the models to date. While this is an appropriate choice when the main interest is in using lake ice phenology as a climate variable, this approach has the potential to inadequately predict ice onset in a littoral zone which is likely to freeze well before ice is observed over the main body of the lake.

In order to improve ice predictions for lakes with littoral zones, we investigate the impact of thermally-driven exchange on the ice onset time of the littoral zone of a freshwater lake. Our focus is given to cooling around and below T_{md}, and the role that the non-linearity in the equation of state might play in determining the strength of the exchange flow. We derive a simple box model which describes the time-rate of change of basin-averaged temperature motivated by observations made at Base Mine Lake (BML) in Alberta, Canada. Our results can be regarded as an initial step in understanding the role of differential cooling around and below T_{md} on the timing of ice onset in a littoral zone.

We begin in section 2 with the derivation of the governing equations describing the cooling during fall turnover for a lake with a littoral zone and a main basin. In section 3, we explore the parameter dependence of our cooling lake model and derive analytical expressions for the time at which a littoral zone will begin to freeze ($t_{f,1}$), the time at which a main basin will begin to freeze ($t_{f,2}$), and the temperature difference between the main basin and the littoral zone at the littoral zone ice-onset time ($\Delta\theta(t_{f,1})$). In section 4, we discuss our model in the context of a case study lake, Base Mine Lake, before concluding with section 5.

2 Conceptual Model Development

We consider a freshwater lake which freezes in winter following fall turnover. This lake has two distinct basins whose geometry can be approximately represented by the model depicted in figure 1(a–b). Namely, there is a littoral zone of constant depth D_1, length L_1 and width B_1, and a main basin of constant depth D_2, length L_2, and width B_2 where $D_1 < D_2$, $L_1 \leq L_2$, and $B_1 \leq B_2$. Each basin of this lake is assumed to be well mixed through time, even below the temperature of maximum density, T_{md}. We can thus use a basin averaged temperature in place of one with spatial dependence, and define T_1 and T_2 as the basin-averaged temperatures of the littoral zone and main basin, respectively. The temperature of each basin is related to the density via a quadratic equation of state for freshwater under the neglect of pressure effects [e.g. 6, 33],

$$\rho_i = \rho_{md} - \rho_* \left(1 - \frac{T_i}{T_{md}}\right)^2, \tag{1}$$

where the subscript $i = 1$ refers to the littoral zone and $i = 2$ refers to the main basin, ρ_{md} (kg m^{-3}) is the maximum density which is attained at the temperature of maximum density, T_{md} (°C), and $\rho_* = 0.132$ kg m^{-3} is the density anomaly which accounts for the density difference between that at the maximum density (ρ_{md}, occurring at T_{md}) and the freezing temperature of fresh water (ρ_f, occurring at $T = 0$°C). Further details on the density anomaly can be found in [10].

We will assume that heat exchange only occurs at fluid–fluid interfaces in the lake. There are two fluid–fluid interfaces, the first is the surface of the lake with the atmosphere (solid blue line in figure 1a) and the second is the interface between the littoral zone and main basin (dashed black line in figure 1a–b). We will further assume, for simplicity, that the heat flux at the lake–atmosphere interface can be represented by a constant value through time and space, $H_o = const.$. This constant value reflects the average daily heat loss from the lake due to the cumulative sum of all heat incoming and outgoing fluxes at the lake boundaries. That is, H_o represents the sum of all heating (e.g., geothermal effects and solar insolation) and cooling (e.g., net negative heat loss at lake surface during the night) spread out over the

course of a day. Since the lake as a whole is cooling over time during the fall cooling period, we expect H_o during this time to be a loss term. The time rate of change of total heat in each basin can thus be expressed as

$$\dot{E}_1(t) = -H_o L_1 B_1 + H_{ex}(t) D_1 B_1 \tag{2}$$

$$\dot{E}_2(t) = -H_o L_2 B_2 - H_{ex}(t) D_1 B_1, \tag{3}$$

where $\dot{\{\}}$ denotes a derivative with respect to time, $E_i = C_p \rho_i V_i T_i$ (in Joules, J) is the total heat of basin i, H_o (W m^{-2}) is the net heat flux between the lake surface and the atmosphere, and H_{ex} (W m^{-2}) is the net heat flux between the littoral zone and main basin, and $C_p = 4200$ J kg^{-1} °C^{-1} is the heat capacity of fresh water, $V_i = D_i L_i B_i$ is the volume of the basin (m^3).

The first term on the right-hand side of equations (2)–(3) represents the average net heat flux between the lake water surface and the atmosphere for the littoral zone and main basin, respectively. In our model, H_o accounts for both radiative fluxes (short-wave and long-wave) and non-radiative fluxes (evaporation/condensation, precipitation onto the water surface, and effects of inflows and outflows) [18]. The average net water–atmosphere heat flux is a loss term for the lake system during fall turnover. This loss is accounted for in the heat budgets (2)–(3) by defining $H_o > 0$ and making the term as a whole negative. As a first approximation, we have assumed that both the littoral zone and main basin are subjected to the same net outgoing surface heat flux, and that H_o is constant through time, and can thus be regarded as the average net water–atmosphere heat flux for the entire seasonal cooling period leading up to ice onset.

The second term on the right-hand side of equations (2)–(3) represents the net flux of heat between the littoral zone and main basin which couples the heat budgets of the two basins. The exchange of heat between the two basins is achieved via a horizontal free convective process often referred to as an *exchange flow* which is driven by a baroclinic pressure gradient between the two basins. In other words, heat flux at the littoral zone–main basin interface will occur when there is a density difference between the two basins. The density of each basin is dictated by the basin temperature in accordance with equation (1), and thus convective heat transfer between the two basins in our model is thermally driven.

The convective heat flux between the two basins can be considered as an exchange of water between the two basins which is constrained by the width of the littoral zone, B_1. There is a volume flux from the littoral zone to the main basin, $q_1 = u_1 y_1 B_1$, where u_1 is the speed at which water travels from the littoral zone to the main basin and y_1 is the depth of the littoral zone current. Likewise, there is a volume flux from the main basin to the littoral zone, $q_2 = u_2 y_2 B_1$, where u_2 is the speed at which water travels from the main basin to the littoral zone and y_2 is the depth of the main basin current. We assume that changes in the water density associated with cooling lead to negligible volume changes in the entire basin, and thus use conservation of volume in place of conservation of mass similar to [41]. Under the Boussinesq assumption (i.e., $|1 - \rho_1/\rho_2| \ll 1$), we can make the rigid lid approximation and assume that $y_1 + y_2 = D_1$ is constant [21].

The littoral zone current carries water at the temperature of the littoral zone, $T_1(t)$, and the main basin current carries water at the temperature of the main basin, $T_2(t)$. The heat flux due to exchange between the littoral zone and main basin is thus given as

$$H_{ex}(t) = \frac{C_p \rho_{md} u_1 y_1}{D_1} \left(T_2(t) - T_1(t) \right), \tag{4}$$

where we have applied an assumption of incompressibility and volume conservation to simplify further using $u_1 y_1 = u_2 y_2$. In order to solve for $u_1 y_1$ in terms of temperature and the problem geometry, we must consider the underlying hydraulics dictating the convective heat exchange between the two basins.

The step change in depth (and possibly width) at the interface between the two basins (figure 1a–b) acts as a vertical (horizontal) contraction, and we can assume that the location where the exchange should initiate is also a location of internal hydraulic control. Thus, the composite Froude number, G, at this location is unity, the expression for which simplifies under the Boussinesq approximation [e.g., 1, 20] to

$$G^2 = \frac{u_1^2}{|g'|\, y_1} + \frac{u_2^2}{|g'|\, y_2} = 1, \tag{5}$$

where

$$g' = \frac{g}{\rho_2}\left(\rho_2 - \rho_1\right) \approx \frac{g}{\rho_{md}}\left(\rho_2 - \rho_1\right), \tag{6}$$

is the reduced gravity. We have used the absolute value of the difference between the main basin and littoral zone densities in order to strike a balance between the convention that $\rho_2 > \rho_1$ in defining the reduced gravity and our choice of notation, which will not change when the littoral zone is in fact denser than the main basin. Assuming that frictional effects are negligible, it can be shown that at the point of internal hydraulic control, the depth of each layer is equal, i.e., $y_1 = y_2 = \frac{1}{2}D_1$, and thus the velocity of each layer is also equal, $u_1 = u_2 = u_{ex}$. The velocity of the gravity current due to the exchange process at the point of internal hydraulic control can be solved for using (5), giving

$$u_{ex} = \tfrac{1}{2}\sqrt{|g'|\, D_1}. \tag{7}$$

Because heat exchange between the two basins is thermally driven, it is convenient to express the time rates of change of total heat content in the littoral zone and main basin as time rates of change of basin averaged temperature instead. Upon substitution of the definition of total heat content, $E_i = C_p \rho_{md} V_i T_i$, where we now use ρ_{md} in accordance with the Boussinesq approximation, into equations (2)–(3), along with equations (1), (4), (6), and (7), we obtain expressions for the time rates of change of basin averaged temperature for the littoral zone and main basin, given respectively by

$$\dot{T}_1 = -\frac{I_o}{D_1} + \frac{1}{4L_1 D_1}\sqrt{\frac{g\rho_* D_1^3}{\rho_{md}}}\left|\left(\frac{T_1}{T_{md}} - 1\right)^2 - \left(\frac{T_2}{T_{md}} - 1\right)^2\right|^{1/2}(T_2 - T_1) \tag{8}$$

$$\dot{T}_2 = -\frac{I_o}{D_2} - \frac{B_1}{4B_2 L_2 D_2}\sqrt{\frac{g\rho_* D_1^3}{\rho_{md}}}\left|\left(\frac{T_1}{T_{md}} - 1\right)^2 - \left(\frac{T_2}{T_{md}} - 1\right)^2\right|^{1/2}(T_2 - T_1) \tag{9}$$

where $I_o = H_o/(\rho_{md} C_p)$ (°C m s^{-1}) is the kinematic heat flux from the lake surface to the atmosphere. Equations (8)–(9) form a system of two coupled ordinary differential equations (ODEs) and are subject to the initial conditions $T_1(0)$ and $T_2(0)$.

Firstly, when $(T_1/T_{md} - 1)^2 = (T_2/T_{md} - 1)^2$, the second term related to exchange on the right hand side of equations (8) and (9) is zero, and the outgoing surface heat flux will more rapidly cool the littoral zone relative to the main basin. This differential cooling process is thus particularly important for establishing density differences between the two basins. Secondly, the impact of the heat flux due to exchange between the two basins will be larger for the littoral zone, even if the littoral zone and main basin have the same surface areas. This is again due to the difference in depth between the two basins and that $D_1 < D_2$. This difference in impact will only be exacerbated by differences in the surface areas of the two basins. Lastly, there are two ways by which the exchange heat flux does not affect the total heat in either basin. The first is when $T_1 = T_2$, which, disregarding any implication this has on the nature of the exchange flow itself, makes perfect sense given that any exchange when

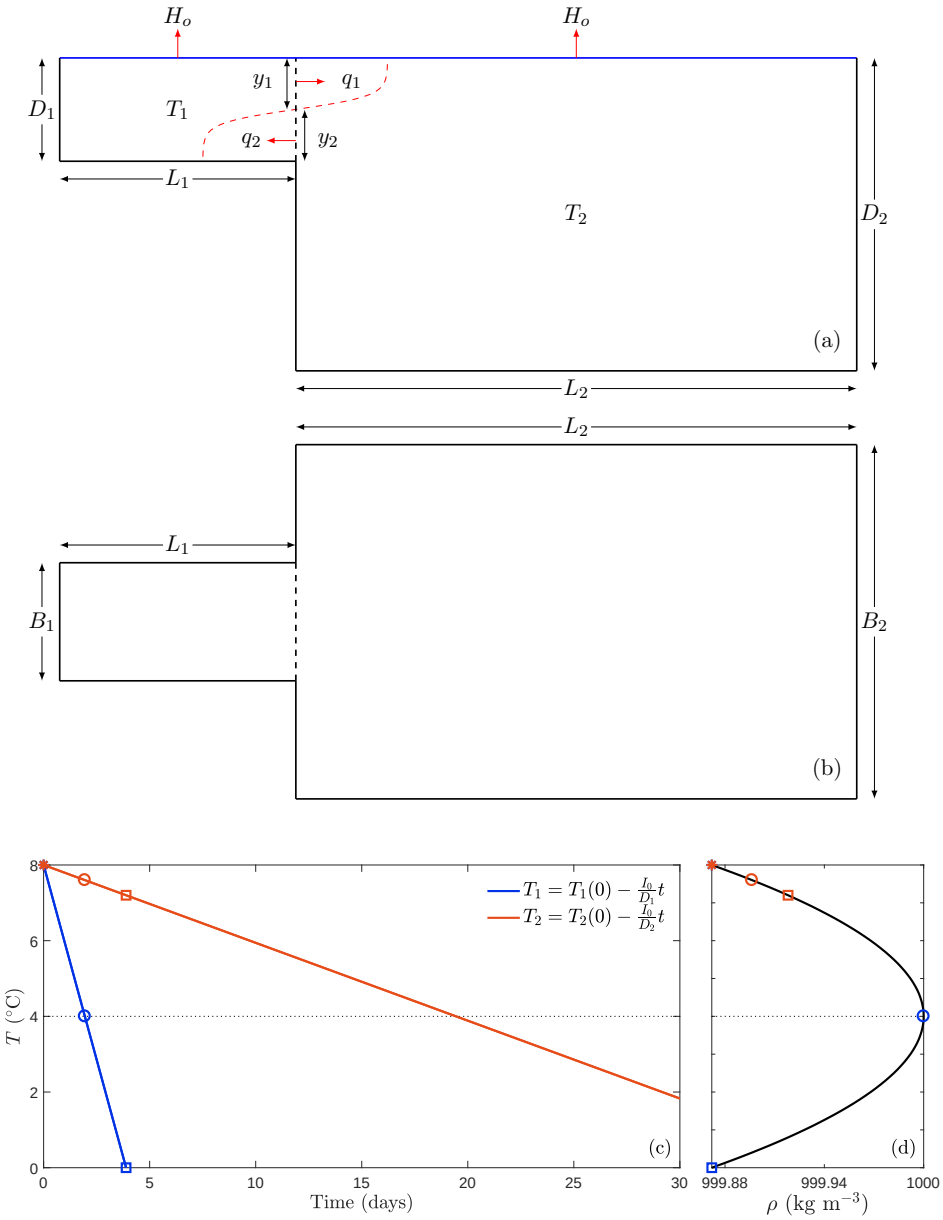

Figure 1: (a) Elevation schematic and (b) bird's eye schematic of the model lake. D_2, L_2, and B_2 are the depth, length, and width of the main basin, respectively. D_1, L_1, and B_1 are the depth, length, and width of the littoral zone, respectively. H_o is the constant and uniform outgoing heat flux from the lake to the atmosphere. T_1 is the temperature of the littoral zone, and T_2 is the temperature of the main basin. A simple sketch of the exchange between the littoral zone and main basin is shown in panel (a) for the example where the main basin is denser than the littoral zone. The depths of the exchange flow gravity currents travelling from the littoral zone to the main basin and vice versa are given by y_1 and y_2, respectively; q_1 and q_2 are the water volume fluxes from the littoral zone to the main basin and the main basin to the littoral zone, respectively; the dashed red line is a simple sketch to aid in visualisation of the direction of the exchange of heat between the two basins. Panels (c) and (d) show an example temperature time series and associated density at selected snapshots, respectively, for a littoral zone (solid blue line) and main basin (solid orange line) which are cooling due to a constant and uniform surface heat flux in the absence of exchange.

$T_1 = T_2$ would result in a net zero change in temperature between the two basins. The second is when $(T_1/T_{md} - 1)^2 = (T_2/T_{md} - 1)^2$, which is when $\rho_1 = \rho_2$. Obviously, $\rho_1 = \rho_2$ when $T_1 = T_2$, but because of the quadratic dependence on temperature of the equation of state for fresh water, so long as T_1 and T_2 are equidistant from T_{md}, $\rho_1 = \rho_2$, and there will be no exchange flow to enable an exchange of temperature.

It is advantageous to non-dimensionalise (8)–(9) in order to better investigate the parameter dependence of this lake cooling model. Let $\widetilde{t} = t/\tau$ be the nondimensional time, where $\tau = D_1 T_{md}/I_o$ is the freezing onset time for the littoral zone in the absence of exchange with the main basin, $\theta_i = (T_i/T_{md} - 1)$ be the non-dimensional temperature, and $\hat{\rho}_i = (\rho_i - \rho_{md})/\rho_* = -\theta_i^2$. Upon substitution, we obtain the non-dimensional set of coupled ODEs

$$\dot{\theta}_1(t) = -1 + \frac{\frac{1}{4} T_{md}\sqrt{g'_* D_1^3}}{I_o L_1} \left|\theta_1(t)^2 - \theta_2(t)^2\right|^{1/2} (\theta_2(t) - \theta_1(t)) \tag{10}$$

$$\dot{\theta}_2(t) = -\frac{D_1}{D_2} - \left(\frac{B_1 L_1 D_1}{B_2 L_2 D_2}\right) \frac{\frac{1}{4} T_{md}\sqrt{g'_* D_1^3}}{I_o L_1} \left|\theta_1^2(t) - \theta_2^2(t)\right|^{1/2} (\theta_2(t) - \theta_1(t)), \tag{11}$$

where $g'_* = g\rho_*/\rho_{md}$ is the reduced gravitational acceleration scale based upon the density anomaly of fresh water, ρ_*, and we have dropped the tilde on time. There are three parameters in this problem, the depth ratio of the littoral zone and main basin, $\delta = D_1/D_2$, the surface area ratio of the littoral zone to that of the main basin, $\alpha = B_1 L_1/B_2 L_2$, and a ratio of the total heat flux per unit width due to exchange at the g'_* scale to that due to loss to the atmosphere in the littoral zone,

$$\Phi = \frac{\frac{1}{4} T_{md}\sqrt{g'_* D_1^3}}{I_o L_1}. \tag{12}$$

In terms of these parameter definitions, the non-dimensional coupled ODEs representing the time rate of change of temperature in the littoral zone and main basin are

$$\dot{\theta_1}(t) = -1 + \phi(t) \tag{13}$$

$$\dot{\theta_2}(t) = -\delta\,(1 + \alpha\phi(t)) \tag{14}$$

respectively, subject to the initial condition

$$\theta_1(0) = \theta_2(0) = \theta_0 \tag{15}$$

where,

$$\phi(t) = \Phi \left|\theta_1(t)^2 - \theta_2(t)^2\right|^{1/2} (\theta_2(t) - \theta_1(t)) \tag{16}$$

is the non-dimensional time-dependent heat flux due to exchange between the littoral zone and main basin. We solve the system defined by (13)–(16) both numerically and using analytical techniques. Numerical solutions were computed with a specified relative and absolute error tolerance of 1×10^{-12} using MATLAB's `ode45` solver, which is based on an explicit Runge-Kutta formula [37].

Our present analysis focuses on an initial isothermal lake condition, θ_0, as it can be assumed that $\theta_1(0) \geq \theta_2(0)$. This is because systems that differentially cool also differentially warm, meaning that at the start of seasonal cooling, shallower regions can be assumed to be warmer than deeper regions, if not at the same temperature. In the case where $\theta_1(0) > \theta_2(0)$, due to differential cooling, there will be some time t_0 at which $\theta_1(t_0) = \theta_2(t_0) = \theta_0$, making the initial isothermal condition the most general initial condition for a seasonally cooling lake and justifying a restriction of the initial condition parameter space.

The dynamics of a differentially cooling lake around and below θ_{md} are elegantly represented by the coupled system of nonlinear ODEs given by (13)–(16) subject to the initial condition $\theta_1(0) = \theta_2(0) = \theta_0$. The cooling of both the littoral zone and main basin is due to a constant and uniform surface heat flux (first term on the right-hand sides of (13) and (14)), and a time-dependent heat flux due to exchange between the littoral zone and main basin (second term on the right-hand sides of (13) and (14)). For a fixed value of Φ, the strength of the exchange flow heat flux depends upon the temperature difference between the two basins, $\theta_2 - \theta_1$, and the non-dimensional speed of the exchange related gravity currents, $|\theta_1^2 - \theta_2^2|^{1/2}$. The combined effect of the heat flux ratio, Φ, the speed of the exchange-related gravity currents, $|\theta_1^2 - \theta_2^2|^{1/2}$, and the temperature difference between the two basins, $\theta_2 - \theta_1$, makes up the total exchange-flow related heat flux, $\phi(t)$.

The depth ratio between the littoral zone and main basin is represented by the parameter δ, and their surface area ratios is represented by the parameter α. While δ affects the overall cooling rate of the main basin with respect to the littoral zone, the influence of α is only observed in the relative importance of the time dependent exchange heat flux, $\phi(t)$, to the cooling rate of the main basin. When $\alpha \ll 1$, the impact of exchange on the cooling in the main basin is effectively negligible. When $\delta \ll 1$, as is the case by definition of our littoral zone, the main basin is effectively decoupled from the littoral zone, and the leading order cooling regimes can be defined from the perspective of the littoral zone. Both the sign and the magnitude of ϕ are of importance. When $\phi > 0$, the littoral zone is cooler than the main basin ($\theta_1 < \theta_2$), and thus exchange with the main basin acts to slow the cooling rate in the littoral zone. Conversely, when $\phi < 0$, the littoral zone is warmer than the main basin ($\theta_1 > \theta_2$), and any exchange with the main basin acts to increase the rate of cooling in the littoral zone. For the purposes of the present paper, we will focus on the situations where the littoral zone is never warmer than the main basin, i.e., $\phi(t) \geq 0$.

For $\phi(t) \geq 0$, there are two basic cooling regimes (i.e., $\dot{\theta}_1(t) \leq 0$) for the littoral zone according to (13). When $\phi(t) \ll 1$, exchange with the main basin is very weak and the rate of cooling in the littoral zone is dominated by the outgoing surface heat flux. When $\phi(t) \approx 1$, exchange with the main basin warms the littoral zone at a rate commensurate with the cooling due to surface heat loss and the littoral zone cools in a quasi-steady state with the main basin. When $\phi(t) \gg 1$, exchange with a warmer main basin overcomes cooling due to surface heat loss, and the littoral zone actually warms (i.e., $\dot{\theta}_1(t) > 0$). However, this warming regime is only possible under extreme initial conditions not considered here. For the cooling lake systems considered by the analysis here, only cooling in the weak exchange and quasi-steady state regimes are of practical importance.

To illustrate the two cooling regimes, the solution to the system (13)–(14) subject to the initial conditions $\theta_1(0) = \theta_2(0) = 1$ at set parameter values $\Phi = 10$ and $\alpha = \delta = 0.1$ is shown in figure 2. In this example solution, the littoral zone begins cooling in the weak exchange regime during which it cools at a rate commensurate with that dictated by the surface heat loss alone ($\dot{\theta}_1 \approx -1$). As the littoral zone rapidly cools in relation to the main basin, the density difference between the two basins grows (figure 2b), leading to the development of weak exchange with the main basin and thus a growth in the magnitude of the exchange related heat flux, $\phi(t)$ (see figure 2d). Once a large enough density difference between the two basins is established, the littoral zone cooling transitions to quasi-steady cooling regime wherein the littoral zone cools in a quasi-steady state with the main basin. Because both the littoral zone and main basin are still above θ_{md}, the quasi-steady cooling regime is interrupted by the littoral zone's passage through θ_{md} which allows the two basins to once again attain the same density, despite now being at different temperatures (figure 2). During this transition period, the exchange flow slows down and shuts off, causing the littoral zone to decouple from the main basin and cool in the weak exchange regime at a rate $\dot{\theta}_1 \approx -1$ again. Further cooling

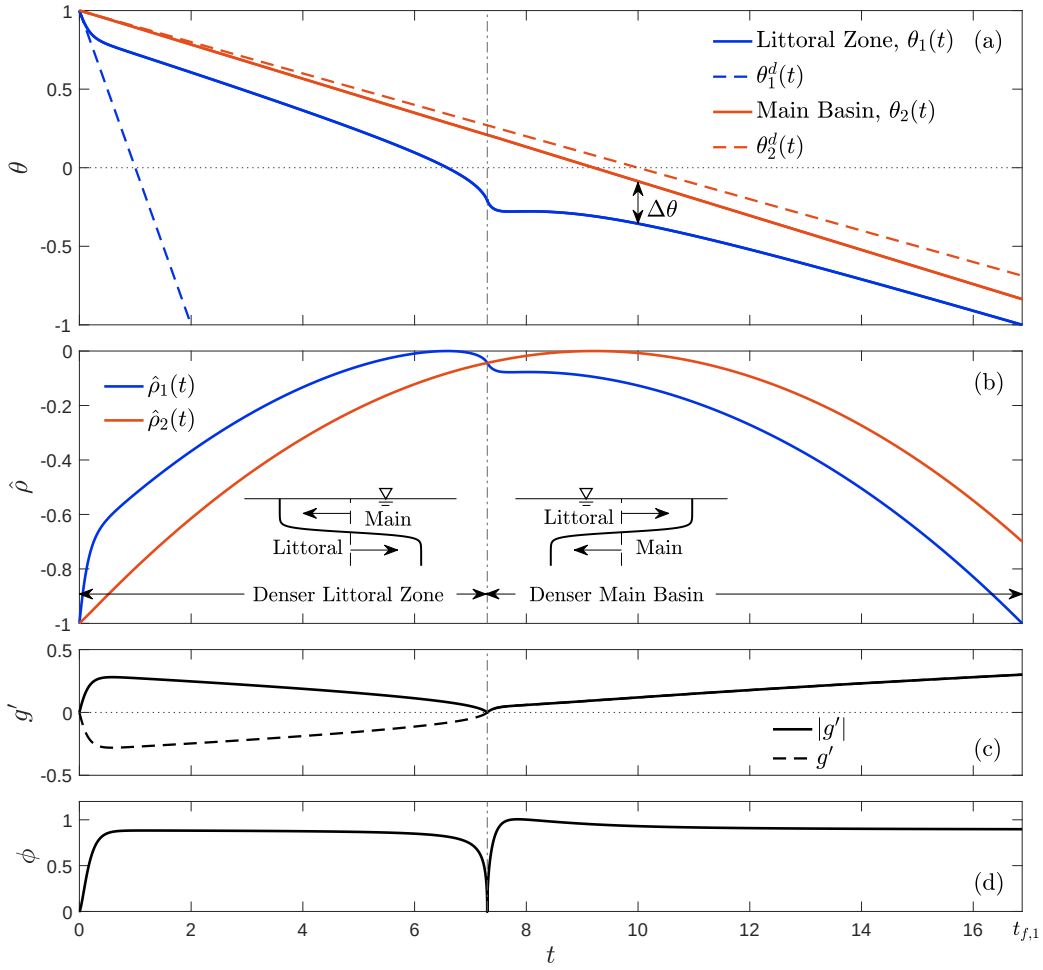

Figure 2: Differential cooling behaviour of a freshwater lake when both the littoral zone and main basin begin cooling from $\theta_i = 1$, the depth ratio $\delta = 0.1$, the surface area ratio $\alpha = 0.1$, and the heat flux ratio $\Phi = 10$. The time evolution of (a) nondimensional temperature ($\theta_i = (T_i - T_{md})/T_{md}$), (b) nondimensional density ($\hat{\rho}_i = (\rho_i - \rho_{md})/\rho_* = -\theta_i^2$, (c) nondimensional reduced gravity ($g' = \hat{\rho}_2 - \hat{\rho}_1$), and (d) nondimensional exchange related heat flux $\phi(t) = \Phi\Delta\theta\sqrt{|g'|}$ are shown. As a point of comparison, the solutions for the temperature in the littoral zone and main basin in the absence of exchange, $\theta_1^d(t)$ and $\theta_2^d(t)$, respectively, are shown as dashed lines in panel (a). The time-axes of panels (a)–(d) span $t = 0$ to $t = t_{f,1}$, where $t_{f,1}$ is the time of ice-onset in the littoral zone defined as when $\theta_1(t_{f,1}) = -1$. The time at which the direction of the exchange circulation changes is indicated as a dash-dotted line in panels (a)–(d), and occurs when g' changes sign. Schematics of the exchange circulation direction are given in panel (b).

of the littoral zone after the shut-down of the exchange flow now decreases the density of the littoral zone relative to the main basin, which re-establishes a baroclinic pressure gradient between the two basins and thus restarts exchange with the circulation changing direction, as seen by the change in the sign of g' (dashed black line in figure 2c). Once the exchange flow is re-established, the littoral zone continues cooling in a quasi-steady state with the main basin until the onset of freezing (2).

As expected, cooling within the weak exchange regime is associated with minima in $|g'|$ (solid black line in figure 2c), which occurs due to the initial conditions of the system ($\theta_1(0) = \theta_2(0)$), and when the temperatures of the two basins become equidistant from T_{md} (see dash-dotted vertical line indicated in figures 2a and b). Likewise, cooling within quasi-steady regime occurs when $\phi(t) \approx 1$ (figure 2d). Notably, after the second transition from the weak exchange regime to the quasi-steady cooling regime, around $t = 7$, cooling in the littoral zone seems to stagnate completely. However, $\phi(t)$ reaches a maximum just past 1 before settling at a value around $\phi(t) \approx 0.9$ until the littoral zone reaches the freezing temperature of fresh-water.

3 Parameter Dependence and Analytical Predictions

The time evolution of the littoral zone and main basin temperatures, $\theta_1(t)$ and $\theta_2(t)$, respectively, are functions of the four governing parameters in the model (13)–(16). These parameters are

1. Φ, the scaled heat flux ratio between the exchange heat flux and surface heat flux in the littoral zone,
2. θ_0, the initial isothermal condition,
3. δ, the ratio of the littoral zone depth to the main basin depth, and
4. α, the ratio of the littoral zone surface area to the main basin surface area.

Our primary focus is on the impact of the governing parameters Φ and θ_0. There are two primary quantities of interest: 1) the timing of ice onset in the littoral zone and main basin, $t_{f,1}$ and $t_{f,2}$, respectively, and 2) the temperature difference between the main basin and the littoral zone at $t = t_{f,1}$, given as

$$\Delta\theta(t_{f,1}) = \theta_2(t_{f,1}) - \theta_{frz}, \tag{17}$$

where by definition of $t_{f,1}$ and $t_{f,2}$, $\theta_1(t_{f,1}) = \theta_2(t_{f,2}) = \theta_{frz}$ where $\theta_{frz} \geq -1$ is the depth averaged temperature at which surface freezing occurs for the lake. We allow flexibility in the value of θ_{frz} because lakes generally experience the onset of surface ice while the depth averaged temperature is above the freezing temperature. For example, in Base Mine Lake (section 4), $\theta_{frz} \approx -0.7$.

In section 3.1 we investigate the model's dependence upon the governing parameters, Φ and θ_0. We show that $\Delta\theta(t_{f,1})$ becomes insensitive to initial lake temperature as the importance of exchange increases relative to the constant surface forcing (i.e., increasing Φ). We demonstrate the model's insensitivity to θ_0 for $\Phi > 1$ and justify the pursuit of an analytical solution to (13)–(16) subject to the initial condition $\theta_0 = 0$ for $\Phi \gg 1$, $\delta \ll 1$, and $\alpha \ll 1$. This analytical solution is derived in appendix B.

In section 3.2.1, we construct predictions for $t_{f,1}$, $t_{f,2}$, and $\Delta\theta(t_{f,1})$ from the analytical solution to (13)–(16) for $\theta_0 = 0$. We then generalise these analytical predictions for any $\theta_0 \geq 0$ in section 3.2.2, subject to the condition that ice onset in the littoral zone occurs during the quasi-steady state cooling period. We compare our analytical predictions to the numerical results and find excellent agreement for $\Phi \gg 1$, $\delta \ll 1$ and $\alpha \ll 1$. We discuss our results in the context of a real-world lake system in section 4.

3.1 Dependence on Φ and Initial Conditions

For illustrative purposes, we will consider the limiting case where $\theta_{frz} = -1$ and set $\delta = \alpha = 0.1$ in our probing of the Φ–θ_0 parameter space. We demonstrate the impact of θ_{frz} on the applicability of our analytical predictions in section 3.2.2. Figure 3 showcases the combined effect of the heat flux ratio, Φ, and the temperature of the lake at the start of seasonal cooling, $\theta_1(0) = \theta_2(0) = \theta_0$ on (a) the timing of ice onset in the littoral zone, $t_{f,1}$, (b) the timing of ice onset in the main basin, $t_{f,2}$, (c) the ice onset time lag between the two basins, Δt_f, and (d) the temperature difference between the two basins when the littoral zone experiences ice onset, $\Delta\theta(t_{f,1})$.

To better understand how Φ affects $\Delta\theta(t_{f,1})$, it is instructive to first consider the limiting case of no exchange ($\Phi = 0$). At $\Phi = 0$, $\phi(t) = 0$ for all t, and the two basins are decoupled because there is no exchange. The model (13)–(14) simplifies to

$$\dot{\theta}_1^d = -1 \tag{18}$$

$$\dot{\theta}_2^d = -\delta, \tag{19}$$

where the superscript d is used to denote this completely decoupled case. When the two basins are completely decoupled, they both cool at a linear rate dictated by their depth and the strength of the surface forcing. From (18)–(19), the decoupled ice onset times for the littoral zone and main basin are

$$t_{f,1}^d = \theta_0 - \theta_{frz} \tag{20}$$

$$t_{f,2}^d = \frac{1}{\delta}\left(\theta_0 - \theta_{frz}\right), \tag{21}$$

respectively. The temperature difference at the ice onset time in the littoral zone is given by

$$\Delta\theta^d(t_{f,1}^d) = (1-\delta)\left(\theta_0 - \theta_{frz}\right), \tag{22}$$

which is shown as circles with colours corresponding to θ_0 in figure 3(d). In this decoupled scenario, where $\Phi = 0$, the difference in temperature between the two basins at $t_{f,1}^d$ is dictated by the difference in depth between the two basins and the initial temperature of the system. As an example, if $\delta = 0.5$, it will take the main basin twice as long to cool from θ_0 to the freezing temperature of fresh water because the main basin cools at half the rate of the littoral zone.

At a small, but finite Φ, exchange processes have the capacity to impact the cooling of the littoral zone, but this depends upon the initial state of the lake. When the two basins start at the same initial temperature, the cooling behaviour will start in the weak exchange regime, which is characterised by rapid cooling of the littoral zone relative to the main basin. It is useful to recall that during the weak exchange regime,

$$\phi(t) = \Phi\left(\theta_1^2(t) - \theta_2^2(t)\right)^{1/2}\left(\theta_2(t) - \theta_1(t)\right) \ll 1, \tag{23}$$

meaning that the main basin and the littoral zone must attain a larger temperature (and density) difference in order for exchange processes to become important to the cooling of the littoral zone when $\Phi \ll 1$. Thus, if θ_0 is close enough to θ_{frz}, it is possible for the littoral zone to experience ice onset before the system transitions to a quasi-steady regime. Conversely, if the lake begins cooling from a temperature which is far enough from θ_{frz} (and θ_{md}), there will be enough time for the rapid littoral zone cooling of the weak exchange regime (weak coupling with the main basin) to establish a strong enough density difference with the main basin for the system to transition to the quasi-steady cooling regime.

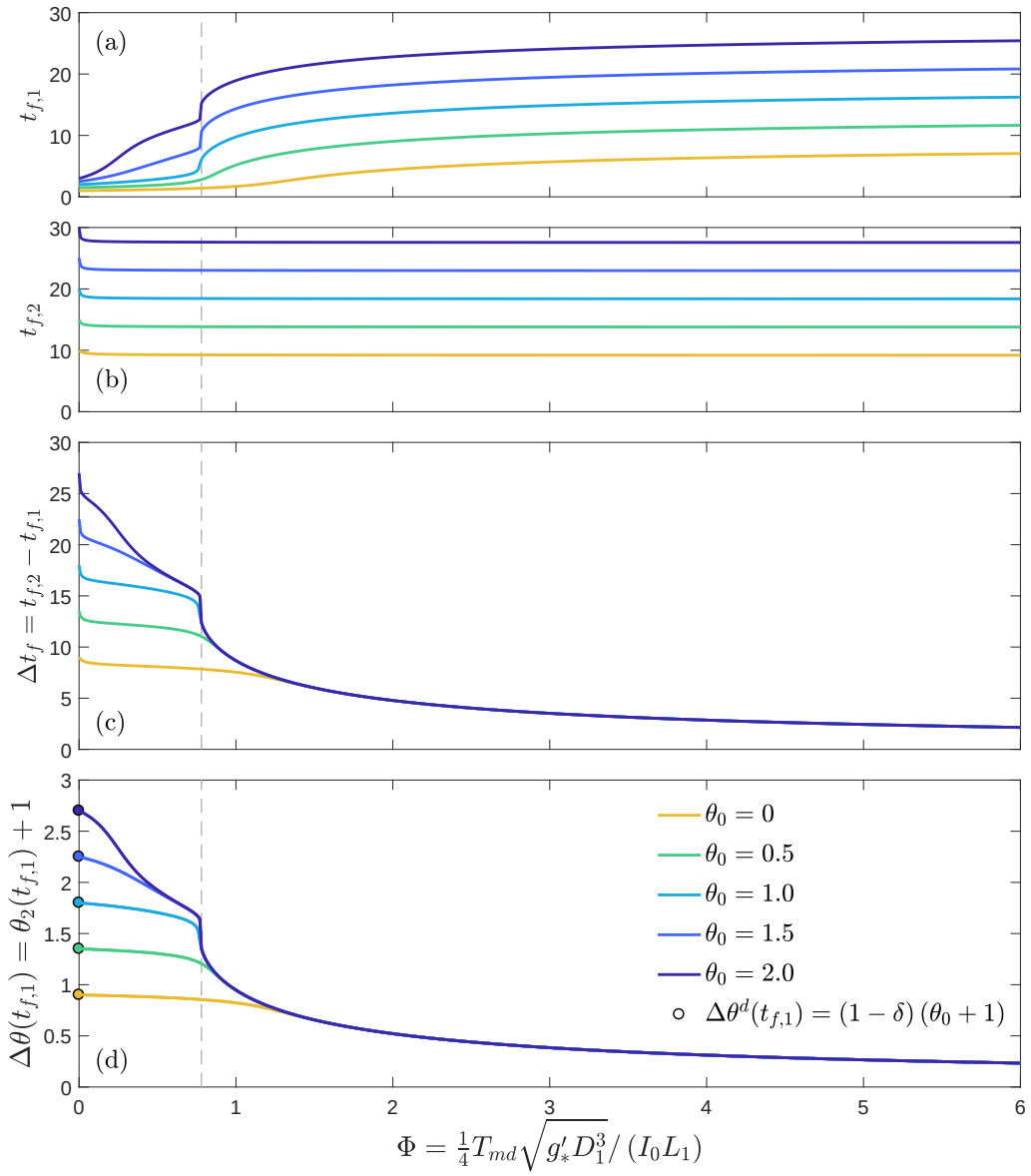

Figure 3: Ice onset time and temperature difference between basins as a function of both the heat flux ratio, $\Phi = \frac{1}{4}T_{md}\sqrt{g'_* D_1^3}/(I_o L_1)$, and the initial lake temperature θ_0, for the illustrative depth ratio $\delta = 0.1$ and surface area ratio $\alpha = 0.1$. The numerical solutions for (a) the ice onset time in the littoral zone, $t_{f,1}$, (b) the ice onset time in the main basin, $t_{f,2}$, (c) the ice onset time lag between the main basin and littoral zone, $\Delta t_f = t_{f,2} - t_{f,1}$, and (d) the temperature difference between the main basin and littoral zone at the ice onset time in the littoral zone, $\Delta\theta(t_{f,1}) = \theta_2(t_{f,1}) + 1$. All solutions have been computed for the limiting case where the basin averaged temperature at which ice onset occurs is $\theta_{frz} = -1$. The predictions for $\Delta\theta(t_{f,1})$ in the zero-exchange limit ($\Phi = 0$), $\Delta\theta^d(t_{f,1})$ given by (22), are shown as solid circles on the $\Phi = 0$ axis.

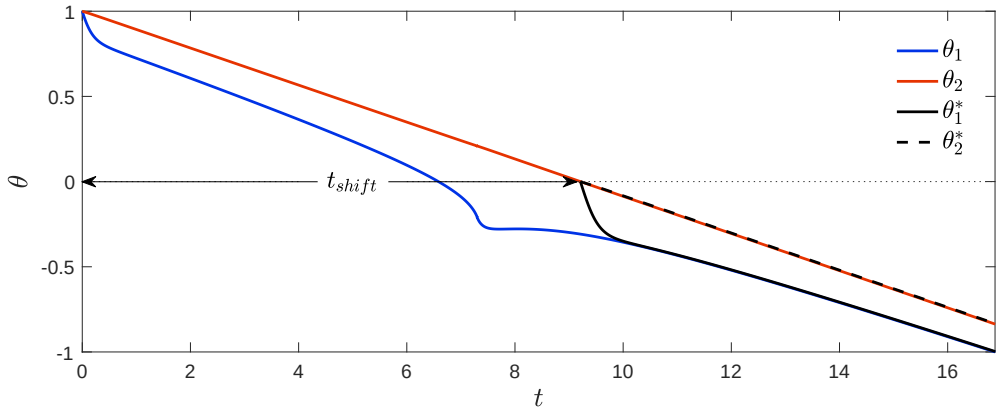

Figure 4: Illustration of the loss of sensitivity to initial conditions when the heat flux ratio, Φ, is sufficiently large. This example is for $\Phi = 10$, a depth ratio $\delta = 0.1$ and a surface area ratio $\alpha = 0.1$. Solutions to the governing equations, (13)–(16), for the initial conditions $\theta_0 = 1$, and $\theta_0 = 0$ are shown for comparison. The solutions $\theta_1(t)$ (solid blue line) and $\theta_2(t)$ (solid orange line) show the cooling in the littoral zone and main basin, respectively, from an initial non-dimensional temperature $\theta_0 = 1$. The solutions $\theta_1^*(t+t_{shift})$ (solid black) and $\theta_2^*(t+t_{shift})$ (dashed black) show the time-shifted cooling in the littoral zone and main basin, respectively, from an initial non-dimensional temperature $\theta_0 = 0$. The time shift, t_{shift}, applied is the time that it takes the main basin to cool to the temperature of maximum density, $\theta_{md} = 0$, which depends linearly on the initial condition according to (32). For the example shown, t_{shift} is the amount of time it takes the main basin to cool from $\theta_2(0) = 1$ to $\theta_2(t_{shift}) = 0$, or $t_{shift} \approx 9.5$.

Increases in Φ correspond to a decrease in both the ice onset time lag (figure 3c) and the temperature difference between the littoral zone and main basin at $t_{f,1}$ (figure 3d). Since the main basin is effectively decoupled from the littoral zone at all times (valid for $\delta \ll 1$, $\alpha \ll 1$, and $\Phi \ll 1/(\delta\alpha)$), a decrease in $\Delta\theta(t_{f,1})$ can be interpreted as an increase in the amount of time that it takes the littoral zone to experience ice onset compared to the completely decoupled case ($\Phi = 0$). This behaviour is clearly shown in figure 3a. Additionally, there is a clear loss of sensitivity to initial conditions with increasing Φ, with no observable effect of $\theta_0 \geq 0$ on Δt_f or $\Delta\theta(t_{f,1})$ for $\Phi > \Phi_{thresh} = 1.3$ (figure 3c–d). This threshold value of Φ, Φ_{thresh}, changes depending upon the range of initial conditions under consideration. This threshold value also has a lower bound, which for $\theta_{frz} = -1$ is approximately $\Phi_{thresh} \approx 0.78$, shown as a dashed grey line in all panels of figure 3.

The existence of the threshold value, Φ_{thresh}, above which Δt_f and $\Delta\theta(t_{f,1})$ become insensitive to the initial state suggests that we can solve for the Φ dependence for all $\Phi > \Phi_{thresh}$ of the system, (13)–(14), subject to the simplest initial condition at fixed δ and α. In this case, the simplest initial state is cooling the system from T_{md}, *i.e.*, $\theta_1(0) = \theta_2(0) = 0$, which we address in the following section. As a proof of concept, we compare the solution to (13)–(14) cooled from $\theta_1(0) = \theta_2(0) = 1$, $\theta_1(t)$ (solid blue line) and $\theta_2(t)$ (solid orange line), to the time-shifted solution to (13)–(14) cooled from $\theta_1(0) = \theta_2(0) = 0$, θ_1^* (solid black) and θ_2^* (dashed black line), in figure 4. The time-shift, t_{shift}, is defined as the time at which the main basin reaches the temperature of maximum density ($\theta_2(t_{shift}) = \theta_{md}$).

As shown in figure 4, the numerical solution to (13)–(14) cooled from $\theta_0 = 1$, $\theta_1(t)$, agrees remarkably well with the time-shifted numerical solution, θ_1^*. This suggests that if one knows the solution to (13)–(14) cooled from $\theta_1(0) = \theta_2(0) = 0$, and how to predict the time shift for

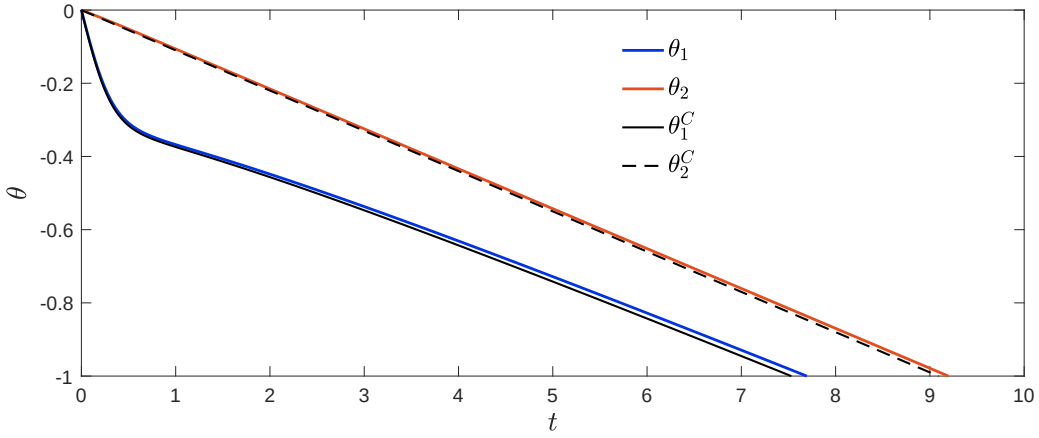

Figure 5: Numerical solutions θ_1 (solid blue line) and θ_2 (solid orange line) to the governing equations (13)–(16) for $\theta_0 = 0$, $\Phi = 10$, and $\delta = \alpha = 0.1$. The comparative analytical composite solutions for the littoral zone (θ_1^C, given by (24)), and main basin (θ_2^C, given by (25)) are shown as solid and dashed black lines, respectively.

a change in initial state of the system, then one can predict the ice onset time in the littoral zone for all initial states. This agreement, however, only occurs when both $\theta_1(t)$ and $\theta_1^*(t)$ are cooling in a quasi-steady state with the main basin. This suggests that use of θ_1^* and an appropriate time-shift will only work when ice onset occurs at a temperature near enough to the freezing temperature so that the non-linearity in the littoral zone solution is avoided altogether (see $5 < t < 10$ in figure 4). This particular condition on θ_{frz} is discussed in more detail in section 3.2.

3.2 Analytical Predictions

The solution to the governing equations (13)–(16) subject to the initial condition $\theta_0 = 0$ for $\Phi \gg 1$, $\delta \ll 1$, and $\alpha \ll 1$ is given by

$$\theta_1^C(t) = \theta_2^C(t) - \Phi^{-1/2}\left(\tanh \Phi^{1/2} t - 1\right) - \Phi^{-2/3}\left(\Phi^{-1/2} - 2\theta_2^C(t)\right)^{-1/3}, \tag{24}$$

$$\theta_2^C(t) = -\delta\,(1+\alpha)\,t. \tag{25}$$

The solution, (24)–(25), is a composite of the solution to an initial weak exchange regime, $\theta_1(t) = \theta_1^W(t)$ and $\theta_2(t) \approx 0$, and the solution to the quasi-steady state regime, $\theta_1(t) = \theta_1^Q(t)$ and $\theta_2(t) = \theta_2^Q(t)$, the details of which can be found in Appendix B.

The solution, (24)–(25), for $\theta_0 = 0$, $\Phi = 10$, and $\delta = \alpha = 0.1$ are compared against the equivalent numerical solution to (13)–(16) in figure 5, showing good agreement. This solution is characterised by an initial period of time during which the system cools in the weak exchange regime ($0 < t < 1$, dotted line in figure B.1) followed by a comparatively longer time period during which the system cools in the quasi-steady state regime ($t > 1$, dot-dashed line in figure B.1). If $\theta_{frz} = -1$, ice onset in the littoral zone occurs during the quasi-steady cooling regime around the non-dimensional time $t = 7.5$. Of note is the apparent divergence of the analytical solutions from the numerical solutions. The degree of divergence around the time of ice onset in the littoral zone is controlled by the magnitude of α, with smaller values of α resulting in better agreement between the numerical and analytical solutions.

3.2.1 Estimating $t_{f,1}$, $t_{f,2}$, and $\Delta\theta(t_{f,1})$

We can construct predictions for the time of ice onset in the littoral and main basin, $t_{f,1}$ and $t_{f,2}$, respectively, and the temperature difference between the two basins at $t_{f,1}$, $\Delta\theta(t_{f,1})$, using the analytical solutions (24) and (25). From (25), the time of ice onset in the main basin is

$$t_{f,2} = \frac{-\theta_{frz}}{\delta\,(1+\alpha)}, \tag{26}$$

where $\theta_{frz} \leq 0$ by definition, making $t_{f,2} > 0$. Since the composite solution for the main basin is a decaying linear function to leading order for all time, there are no restrictions on when the estimate given by (26) is valid. For the littoral zone, however, the cooling regime during which ice onset occurs is vital. Estimation of $t_{f,1}$ is simplified if we assume that ice onset in the littoral zone will occur during the quasi-steady cooling period. This requires that the second term in (24) representing the effects of the weak-exchange regime be negligible, which happens when $\tanh\left(\Phi^{1/2}t\right) \approx 1$. Stated differently, we require that ice-onset in the littoral zone $t_{f,1} \gg \Phi^{-1/2}$, which we will check *a posteriori*. Assuming that this condition on $t_{f,1}$ will be met, we can use the quasi-steady temperature difference between the two basins, $\Delta\theta = \theta_2 - \theta_1$ to our advantage.

During the quasi-steady state regime, the difference in temperature between the two basins is given by

$$\Delta\theta^Q(t) = \theta_2^Q(t) - \theta_1^Q(t) = \left(\Phi^{3/2} - 2\Phi^2\theta_2^Q(t)\right)^{-1/3}, \tag{27}$$

which can be assumed to be approximately constant over time scales which are short enough for $\theta_2^Q(t)$ to be assumed approximately constant. When $\delta \ll 1$, the main basin is approximately decoupled from the littoral zone. This decoupling from the littoral zone means that we can calculate an effective temperature difference between the main basin and littoral zone at the time of ice onset in the main basin, $t_{f,2}$. Using (27), this temperature difference at the time of ice onset in the main basin is given by

$$\Delta\theta^Q(t_{f,2}) = \left(\Phi^{3/2} - 2\Phi^2\theta_{frz}\right)^{-1/3}. \tag{28}$$

If the time lag between ice onset in the littoral zone and that in the main basin, $\Delta t = t_{f,2} - t_{f,1}$, is sufficiently small, we can assume that $\Delta\theta(t_{f,2}) \approx \Delta\theta(t_{f,1})$. We can thus approximate the timing of ice onset in the littoral zone as the time of ice onset in the main basin minus the amount of time it takes the main basin to cool by $\Delta\theta^Q(t_{f,2})$. That is, that $t_{f,1} = t_{f,2} - \Delta t$. According to (28) and (25), it takes the main basin

$$\Delta t = \frac{\left(\Phi^{3/2} - 2\Phi^2\theta_{frz}\right)^{-1/3}}{\delta\,(1+\alpha)} \tag{29}$$

longer than the littoral zone to experience ice onset. Thus, we can approximate the time of ice onset in the littoral zone to be

$$t_{f,1} = \frac{-\theta_{frz} - \left(\Phi^{3/2} - 2\Phi^2\theta_{frz}\right)^{-1/3}}{\delta\,(1+\alpha)}, \tag{30}$$

where, again, $\theta_{frz} < 0$ by definition, making $t_{f,1} > 0$.

The applicability of (30) requires that $t_{f,1} \gg \Phi^{-1/2}$. We can assess whether there are limitations on our prediction given by (30) by considering two possibilities: 1) the depth averaged temperature at which ice-onset occurs is approximately the freezing temperature ($\theta_{frz} \approx -1$) and 2) the depth averaged temperature at which ice-onset occurs is approximately

the temperature of maximum density ($|\theta_{frz}| \ll 1$). In the case that $\theta_{frz} \approx -1$, ice onset in the littoral zone scales as $t_{f,1} \sim \delta^{-1}$. So, to satisfy $t_{f,1} \gg \Phi^{-1/2}$ in this case, we require that $\delta \ll \Phi^{1/2}$. Given that our model is applicable when Φ is sufficiently large and $\delta \ll 1$, this is reasonably met.

For the case that $|\theta_{frz}| \ll 1$, we can first consider $\theta = 0$ as the upper limit on θ_{frz}. In this case, $t_{f,1} < 0$, which is not physically reasonable. If instead $\theta_{frz} = -\Phi^{-1/2}$, $t_{f,1} \approx \frac{1}{3}\delta^{-1}\Phi^{-1/2}$, which is again reasonably met when $\delta \ll 1$. A general requirement is that

$$|\theta_{frz}| \geq \Phi^{-1/2} \tag{31}$$

to ensure that $t_{f,1} > 0$, and thus the applicability of the prediction given by (30).

3.2.2 Generalising $t_{f,1}$, $t_{f,2}$, and $\Delta\theta(t_{f,1})$ for $\theta_0 \geq 0$

The solutions for the ice onset times in the main basin (26) and littoral zone (30) can be generalised to any initial condition $\theta_0 \geq 0$ by adding the time shift, t_{shift} shown in figure 4. This time shift is the amount of time that it takes the main basin to cool from some $\theta_0 \geq 0$ to the temperature of maximum density, $\theta = 0$. This time shift can be found using (25) to be

$$t_{shift} = \frac{\theta_0}{\delta\,(1+\alpha)}, \tag{32}$$

which gives the general solutions for the time of ice onset in the littoral zone and main basin respectively as,

$$t_{f,1} = \frac{\theta_0 - \theta_{frz} - \left(\Phi^{3/2} - 2\Phi^2\theta_{frz}\right)^{-1/3}}{\delta\,(1+\alpha)}, \tag{33}$$

$$t_{f,2} = \frac{\theta_0 - \theta_{frz}}{\delta\,(1+\alpha)}. \tag{34}$$

The time lag in ice onset between the main basin and littoral zone is given by

$$\Delta t_f^Q = t_{f,2}^Q - t_{f,1}^Q = \frac{\left(\Phi^{3/2} - 2\Phi^2\theta_{frz}\right)^{-1/3}}{\delta\,(1+\alpha)}, \tag{35}$$

and the temperature difference between the main basin and littoral zone at the time of ice onset in the littoral zone by

$$\Delta\theta^Q(t_{f,1}) = \left(\Phi^{3/2} - 2\Phi^2\theta_{frz}\right)^{-1/3}. \tag{36}$$

Figure 6 provides a comparison between the analytical and numerical predictions for the ice-onset time lag (panel a) and the temperature difference between the two basins at the time of ice onset in the littoral zone (panel b) as functions of the heat flux ratio, Φ. Both the numerical and analytical solutions were computed for the initial condition $\theta_0 = 1$, the depth ratio $\delta = 0.1$, and the surface area ratio $\alpha = 0.1$. The analytical predictions for both the ice-onset time lag and the temperature difference at ice onset in the littoral zone are denoted by superscript Q, Δt_f^Q (equation 35) and $\Delta\theta^Q(t_{f,1}^Q)$ (equation 36), respectively. The absolute error between the numerical and analytical predictions is shown for four values of ice-onset temperature, $\theta_{frz} = -1$ (solid black line), $\theta_{frz} = -0.5$ (dotted black line), $\theta_{frz} = -0.25$, (dot-dashed black line), and $\theta_{frz} = 0$ (dashed black line).

The importance of θ_{frz} in addition to Φ on the applicability of our analytical solutions is made evident by the poor performance of both $\theta_{frz} = -0.5$ and $\theta_{frz} = -0.25$. For moderate

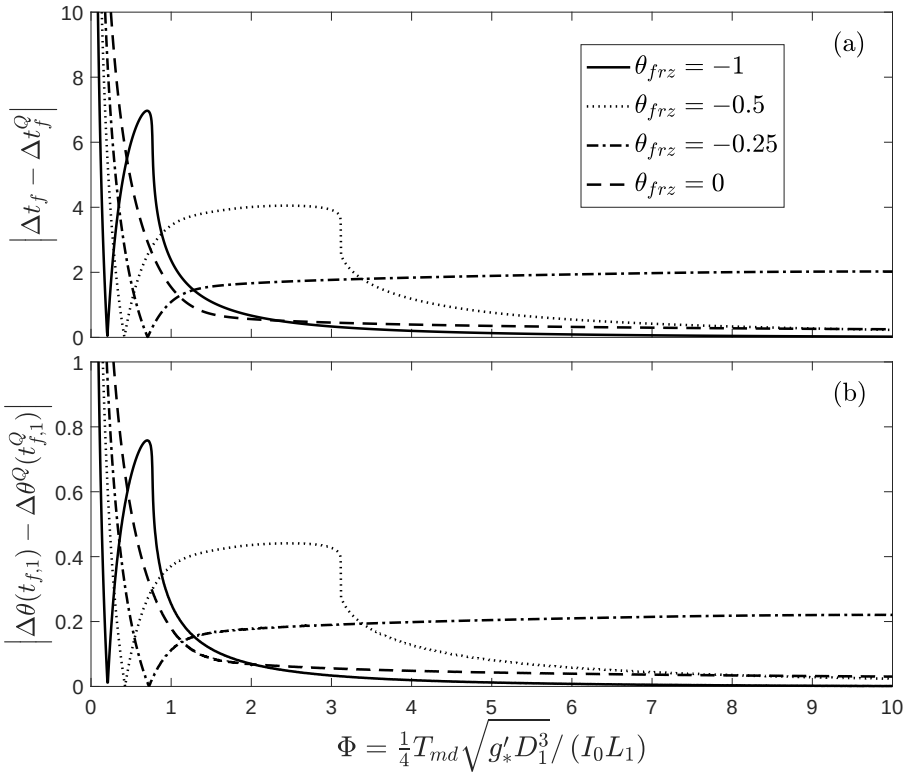

Figure 6: Comparison between numerical solutions and analytical predictions. The absolute errors for (a) the analytical prediction for the ice onset time lag between the main basin and littoral zone, Δt_f^Q, given by (35) and (b) the temperature difference between the main basin and littoral zone at the time of ice onset in the littoral zone, $\Delta\theta(t_{f,1}^Q)$, given by (36) are shown for $\theta_{frz} = -1$, $\theta_{frz} = -0.5$, $\theta_{frz} = -0.25$, and $\theta_{frz} = 0$. Both numerical and analytical computations are made for the illustrative initial condition $\theta_0 = 1$, depth ratio $\delta = 0.1$, and surface area ratio $\alpha = 0.1$.

values of Φ (e.g., $1 \leq \Phi \leq 5$), an ice onset temperature $\theta_{frz} = -0.5$ places ice onset during a period of weak exchange. However, when $\Phi = 10$, as is the case in the examples shown in figures 2 and 4 for $\theta_0 = 1$, an ice onset temperature of $\theta_{frz} = -0.5$ places ice onset during the quasi-steady cooling period. This is reflected by the apparent agreement between the analytical and numerical predictions in both panels of figure 6 at $\Phi = 10$.

The agreement between the analytical solutions given by (35) and (36), however, is poor over the entire $\Phi > 1$ space shown for $\theta_{frz} = -0.25$. This is because there is necessarily a second minimum in g' due to the littoral zone temperature passing through θ_{md} (see figure 2). The impact of Φ is to effectively narrow the period of time during which the system cools in the weak exchange regime, meaning that there are narrower restrictions on the value of θ_{frz} as Φ increases. For the illustrative example shown in figure 2 where $\Phi = 10$, according to (31), the analytical predictions are not applicable for $|\theta_{frz}| < 0.32$, which is reflected in both panels of figure 6.

Notably, the lower bound on Φ_{thresh} discussed at the end of section 3.1 corresponds with the peak in the $\theta_{frz} = -1$ line in figure 6. A sharp decrease in the absolute error between the analytical predictions and the numerical predictions occurs for $\Phi > \Phi_{thresh}$, as expected. Further, it is apparent that the magnitude of Φ_{thresh} depends upon θ_{frz}. Using figure 6, the predicted value of Φ_{thresh} when $\theta_{frz} = -0.5$ and $\theta_0 = 1$ is $\Phi_{thresh} \approx 3.1$.

4 Case Study: Base Mine Lake

We compare our model, (13)–(16), to observations made during fall turnover leading up to ice onset in 2015 at Base Mine Lake (BML) to serve as a basis of discussion of our model and its application to real world systems. BML is a dimictic oil sands end pit lake in the Athabasca oil sands region of Alberta, Canada, and is a site ongoing research [e.g., 5, 17, 40, 47]. The main basin of BML had an average depth of approximately 8 m during fall turnover in 2015 [5], and the littoral zone had an average depth of approximately 1 m (see figure 7a-b). The geometry of BML makes it an ideal case study lake for our model for two reasons, 1) the depths of both the littoral zone and main basin are relatively constant through space and 2) the transition between the littoral zone and main basin is relatively sharp (see sample depth transect shown in figure 7b).

4.1 Methods and Data

In order to apply our model, (13)–(16), to BML, we define representative lengths, widths, and depths for both the littoral zone and main basin of BML, summarised in table 1. These definitions are based off of water level and bathymetry data, both of which were used to render figure 7(a) and (b). We use water temperature measurements taken hourly from the Platform 3 mooring (P3, shown as a black cross in figure 7a) to define a representative dynamic surface heat flux, I_o, during fall turnover, defined as

$$I_o = D_2 \dot{T}_{BML}, \tag{37}$$

where we have assumed that the rate of temperature change in the main basin is constant and uniform, i.e., $\dot{T}_{BML} \approx const.$. We use a linear regression of the depth-averaged temperature to define $\dot{T}_{BML}$, the details of which can be found in [10]. The wind data shown in figure 8(d) was collected 3.33 m above the water surface at Platform 1 (P1, shown as a black open circle in figure 7a).

Table 1: Approximate values of both dimensional and non-dimensional parameters relevant to Base Mine Lake.

Dimensional										**Non-dimensional**		
D_1 (m)	L_1 (km)	B_1 (km)	D_2 (m)	L_2 (km)	B_2 (km)	T_{md} (°C)	$\dot{T}_{BML}$ (°C/s)	H_o (W/m^2)	τ (days)	δ	α	Φ
1	0.3	1.4	8	2.3	3.3	3.7	-3×10^{-6}	-100	1.8	0.13	0.05	4.2

4.1.1 Selection of Initial Time

We initialise the model when the depth averaged temperature of the main basin reaches $T_{BML} = 8$°C on October 25, 2015, as opposed to the start of fall turnover which occurred on September 4, 2015 [5]. There are two reasons for this choice, 1) the cooling rate in the main basin becomes relatively stationary after reaching $T_{BML} = 8$°C, and 2) the temperature of the littoral zone is of negligible importance given that Φ is continuously sufficiently large after October 25. The first point is an assumption of our model, and the second point is related to the insensitivity of our model to the initial conditions. The insensitivity of the model, (13)–(16), at sufficiently large Φ holds even for unequal initial conditions, $\theta_1(0) \neq \theta_2(0)$. This means that so long as our choice of initial time is before the observed ice onset time in the littoral zone and our initial condition in the main basin is well supported, we are free to use any reasonable initial condition for the littoral zone.

As evidenced in figure 7(c), not only is the rate of temperature change fairly constant, but BML remains well mixed even through T_{md}, which is consistent with our assumption that there is enough energy to keep the main basin well-mixed until ice onset. There are two time periods of interest during which noticeable stratification occurs, between 319.0 <DOY< 320.0 and for DOY> 323.0, which as will be seen, are associated with the timing of ice onset in the littoral zone and in the main basin, respectively. The dimensional and associated non-dimensional parameters of BML are summarised in table 1. The depth-averaged temperature time series of the main basin due to a constant and uniform surface heat flux I_o defined by (37) is shown as a dashed red line in figure 7(c) and as a black dashed line in figure 8(a).

4.1.2 Estimation of Ice Onset Time

In order to estimate the timing of ice onset in both the littoral zone and main basin, we rely upon two different datasets. The first is a temperature dataset from the P3 mooring (see figure 7c) and the second is a list of ice-cover classifications based off of images taken of the surface of BML from different angles in November 2015. Five cameras were installed at BML in August 2015, one of which (camera 2), was directed towards the surface of the littoral zone, and four of which (cameras 1, 3, 4, and 5) were directed towards different locations of the main basin. Images were logged hourly during the daylight hours (between 10:00 and 15:00 local time (LT)). To define an ice onset date, we identified the first observation of surface ice that is not followed by a period of open water until the spring melt. Based off of this, ice onset occurred for the littoral zone on November 15 at 15:00 LT (DOY = 319.63). Because of the timing of ice onset in the littoral zone, the uncertainty related to this is approximately one hour. Ice onset in the main basin occurred approximately three and a half days later on November 19 at 10:00 LT (DOY = 323.42). All four cameras angled at the surface of the main basin indicated this ice onset time. The uncertainty related to the estimation of ice

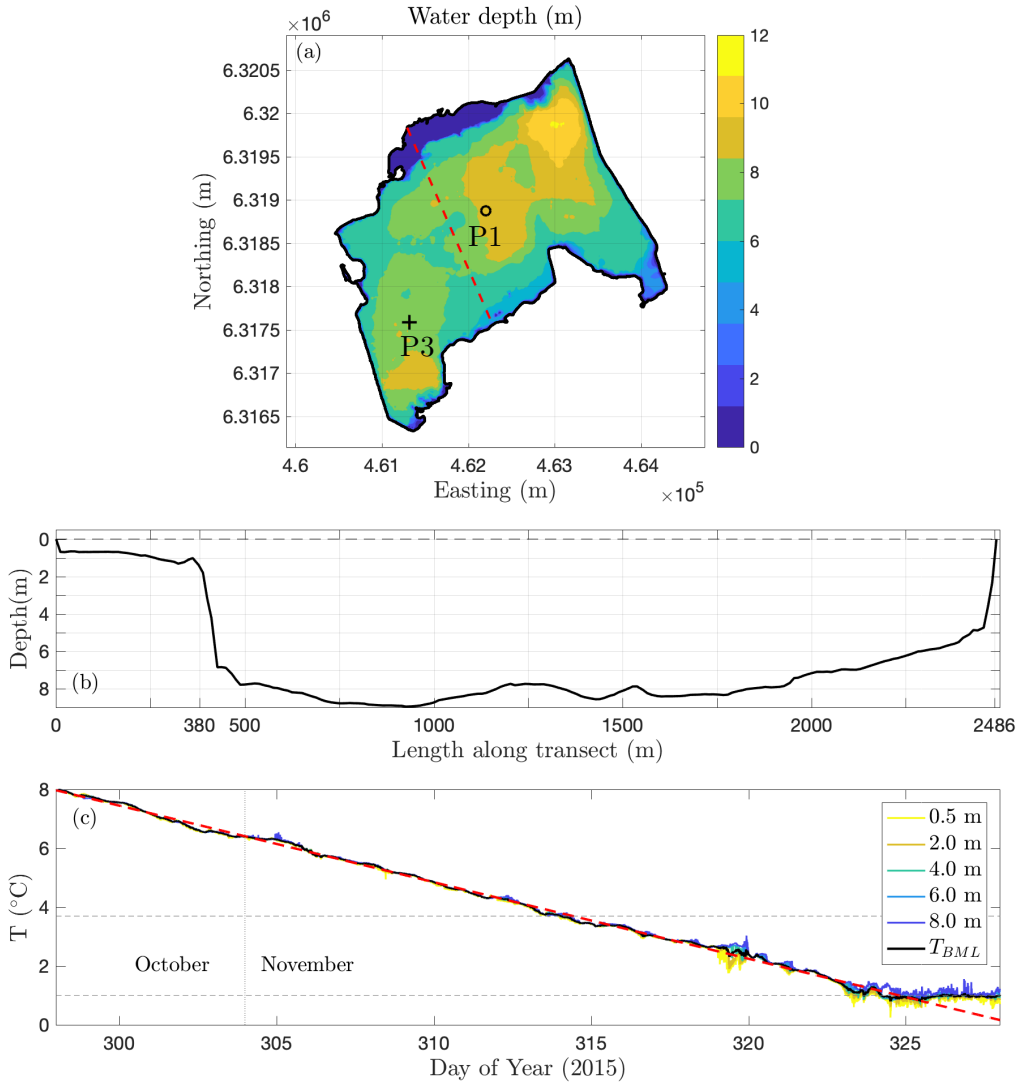

Figure 7: (a) Bathymetry of Base Mine Lake, Alberta, Canada, reflected as contours of water depth (m), (b) water depth (m) along a transect through the littoral zone and the main basin of BML, and (c) time series of temperature observed at data acquisition site P3 with depth at BML during seasonal cooling in 2015. The location of the depth transect shown in panel (b) is indicated as a dashed red line in panel (a). The locations of Platform 1 (P1; black open circle) and Platform 3 (P3; black cross) are shown in panel (a). The arithmetic depth-averaged temperature of the main basin, T_{BML} is shown as a solid black line in panel (c), with an associated linear fit shown as a dashed red line, the slope of which gives $\dot{T}_{BML} = -I_o/D_2$.

onset time in the main basin from the image data is approximately 19 hours.

While there is uncertainty in the ice onset dataset compiled from the hourly images of BML, both the ice onset times in the littoral zone and main basin identified are supported by the P3 mooring data. This gives us a fair amount of confidence in the estimation of ice onset in both the littoral zone and main basin. Around November 19, 2015 (DOY= 323.0), the main basin obviously stratifies and the depth-averaged temperature of the main basin, T_{BML}, settles to a stationary value of approximately 1.1°C (figure 7c). The establishment of stationarity in both T_{BML} and stratification near the freezing temperature of fresh water are clear indications of ice onset in the main basin. While there is no temperature data in the littoral zone, there is an obvious stratification event in the main basin around November 15, 2015 (DOY= 319.0), which indicates that the meteorological conditions at BML at the time were likely favourable for ice onset in the littoral zone (given that it is expected to be cooler than the main basin at this time).

Because ice onset in the main basin occurs when $T_{BML} \approx 1.1$°C, we will define the ice onset temperature for BML as $T_{frz} = 1.1$°C. Since $T_{md} \approx 3.7$°C for BML, the non-dimensional freezing temperature is given as

$$\theta_{frz} \approx -0.703. \tag{38}$$

4.2 Comparison with Model and Discussion

According to the numerical solution to the governing equations, (13)–(16) for $\theta_0 = 1.2$, ice onset in the littoral zone of BML occurs in the evening of November 14 (DOY = 318.65). The uncertainty in this numerical estimate due to our uncertainty in the initial condition of the littoral zone is approximately 11 hours, shown as time error bars in figure 8(a) (see [10] for more details). Comparatively, the analytical prediction for $t_{f,1}$ given by (33) predicts that ice onset in the littoral zone occurs approximately 8 hours later at DOY= 319.03. Both estimates, however, are within a reasonable range for ice onset in the littoral zone. Observations based off of hourly images suggest that littoral zone ice onset occurred at 15:00 on November 15 (DOY= 319.63), and temperature data suggests that ice onset could have reasonably occurred anywhere between 319.0 <DOY< 320.0 (see stratification event in figure 8b). It is likely that the depth-averaged temperature at which the littoral zone experiences ice onset is closer to the freezing temperature of fresh water ($\theta_{frz} = -1$). When we use a value of θ_{frz} closer to $\theta_{frz} = -1$ in the littoral zone, both our numerical and analytical predictions for the littoral zone improve. Given the assumptions necessary to derive the asymptotic prediction for ice onset in a littoral zone, (33), the agreement between the analytical prediction and observations is remarkable.

Given that we force the model (13)–(16) with a surface heat flux, I_0, that is defined using $\dot{\theta}_{BML}$, it is not surprising that the numerical solution $\theta_2(t)$ agrees well with $\theta_{BML}(t)$. Ice onset is predicted to occur on November 19 at 10:00 LT, which exactly agrees with observations.

4.2.1 Assumption of Constant Surface Heat Flux

Our assumption of well-mixedness of each basin through time allows us to combine all incoming and outgoing heat sources and sinks into one net flux at either the top or bottom interface. The surface heat flux, H_o, which we employ here is a representation of the average heat loss from the lake system when considering both cooling processes (e.g., outgoing long-wave radiation from the lake surface) and heating processes (e.g., warming from the bottom sediments and day-time solar insolation).

The cooling and heating processes that H_o represents are themselves functions of time and space. The most pressing time-dependence that is ignored is that of heat loss at the lake-atmosphere surface (e.g., by outgoing long-wave radiation during the nighttime). This

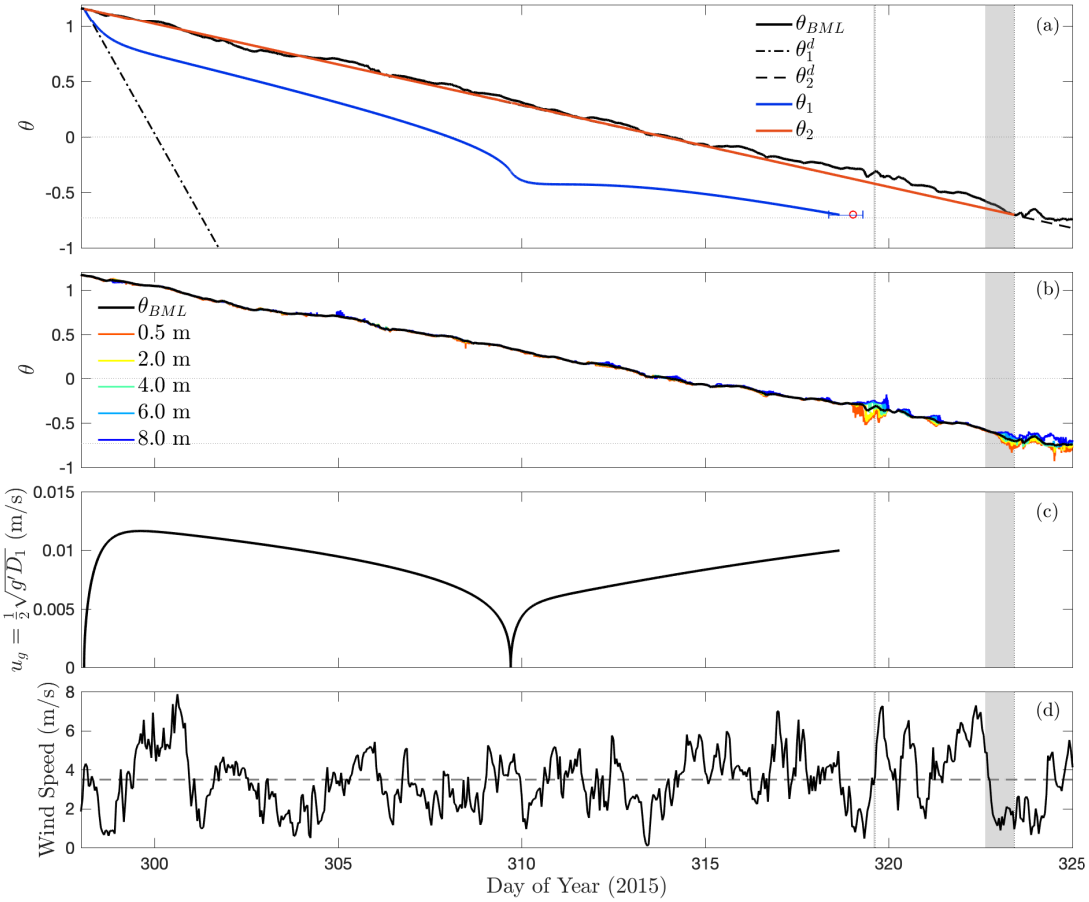

Figure 8: (a) Timeseries of non-dimensionalised temperature in the littoral zone (θ_1; blue line) and main basin (θ_2; orange line) of BML as modelled by the governing equations (13)–(16) for $\Phi \approx 4.2$, $\theta_0 \approx 1.2$, $\delta \approx 0.13$, $\alpha \approx 0.05$, and $\theta_{frz} \approx -0.7$. The decoupled solutions for the littoral zone (θ_1^d; dot-dashed black line) and main basin (θ_2^d; dashed black line) are shown, along with the observed timeseries of depth-averaged temperature at P3 (θ_{BML}; solid black line). The analytical prediction for the timing of ice onset in the littoral zone according to (33) is shown as an open red circle. Error bars are shown for the numerical time of ice onset in the littoral zone for the extreme hypothetical initial conditions where the littoral zone is just above freezing ($\theta_1(0) = -0.7$; lower error) and where the littoral zone does not cool before DOY= 298.0 ($\theta_1(0) = 3$; upper error). (b) Timeseries of observed non-dimensionalised water temperature at P3 at depths 0.5 m (red line), 2.0 m (yellow line), 4.0 m (green line), 6.0 m (cyan line), and 8.0 m (blue line). The depth-averaged temperature timeseries at P3 is also shown (θ_{BML}; black line). Note that the temperature range is 0°C – 8°C, matching figure 7c. (c) Timeseries of the exchange-related gravity current speed in m s^{-1}. (d) Timeseries of hourly wind speed measurements taken at Platform 1 (P1). The average wind speed shown as a dashed grey line is 3.5 m s^{-1}. The observed ice onset times for the littoral zone (DOY= 319.63; November 15 15:00) and main basin (DOY= 323.42; November 19 10:00) are shown in all panels as vertical dotted lines, with the grey shading associated with the uncertainty in each observation based off of data availability.

surface heat flux is driven by the temperature difference between the lake surface and the atmosphere. While our assumption of a constant-in-time surface heat flux between the lake and the atmosphere seems appropriate for BML (evidenced by approximately linear decay of main basin temperature in figure 8b), our assumption that it is constant in space is violated whenever the littoral zone and main basin are of different temperatures.

Under the assumption that lake surface temperature is the only driver behind the net surface heat flux and that the surface temperatures of both basins is greater than the temperature of the atmosphere (which is held constant), then the warmer basin would have a stronger net outgoing surface heat flux. This would mean that when the difference between the two basins is the greatest (i.e., the littoral zone is at its coldest relative to the main basin), the rate of cooling of the littoral zone due to surface heat loss would be slower than what is represented currently by our model. Given that our analytical solutions predict an earlier ice-onset than observed in the littoral zone, it is possible that the non-homogeneity in the surface heat flux due to difference in basin temperatures is an important factor to consider. A full analysis of the impact of a temperature-dependent surface heat flux is needed, however, to fully assess the error our assumption of homogeneous surface heat flux introduces.

4.2.2 Role of Wind

Once a lake has cooled to the temperature of maximum density, additional surface cooling no longer acts as a destabilising surface buoyancy force, and rather becomes a stabilising one. At this point, the role of wind becomes important in that it is now needed to maintain a surface mixed layer [e.g. 41]. While it is clear that there is enough energy input to BML to maintain well-mixedness in the deeper main basin below θ_{md} in a broad sense (see figure 8b), there are still calmer periods during which stratification is observed in the main basin. In particular, around DOY= 321.0, the wind speed decreases to around 2 m s^{-1}, and a weak and short lived stratification event is observed in the main basin (see figure 8b and d). During this very brief period, the depth of the surface mixed layer is less than 4 m.

A change in the depth of the mixed layer indicates a change in the depth ratio, δ, of our model. To accommodate the wind's impact on δ, an effective depth ratio could be used in place of the strictly bathymetry based depth ratio used here. This effective depth ratio would be a function of the wind speed. Consider BML as an example. If the wind is only strong enough to mix to a depth of 5 m, then $\delta = 0.2$ could be used instead of the actual geometrical parameter value of $\delta \approx 0.1$. This would understandably decrease the accuracy of our analytical prediction for ice onset in the littoral zone, (33). There is the further potential to allow a time varying effective depth ratio, but considering how this might change the cooling behaviour in the littoral zone is beyond the scope of this work.

Wind can not only impact the depth of the mixed-layer, but can also impact the strength of the exchange flow between the two basins. Exchange in a shallow confined basin like the one we consider here is more likely to be controlled by both horizontal density gradients and cross-shore wind stresses [e.g., 34], depending, of course, on the wind direction. The wind's impact on exchange is maximised when the wind is directed perpendicular to the interface between the littoral zone and main basin, and minimised when directed parallel to this interface. While wind direction data is not presently available here, approximate bounds on the effect of the wind on the exchange flow can be estimated using the measured wind speed.

Considering the wind's potential to either enhance or inhibit exchange between the two basins, the impact of wind on exchange could be accounted for by either increasing Φ (wind enhanced exchange) or decreasing Φ (wind inhibited exchange). This, however, would not account for any wind-driven exchange that might still occur during the weak exchange cooling regime when thermally-driven exchange becomes negligible. In order to fully accommodate

wind-driven exchange, an additional term could be added to the governing equations (13) and (14), which allows exchange even during periods of negligible thermally-driven exchange, but this too is beyond the scope of the current work.

It is also possible for a thermal bar to develop between the littoral zone and main basin due to differential cooling during periods of weak wind [e.g. 11]. Were a thermal bar to develop, however, the littoral zone may freeze much earlier than what is observed (see Appendix G in [10] for more details). This is because the thermal bar would extend the length of the second period of decoupled cooling effectively allowing the littoral zone to freeze before the eventual disappearance of the thermal bar (or end of cabbeling).

4.2.3 Role of θ_{frz}

The depth averaged temperature at which freshwater lakes experience ice onset varies. The reason behind this being the strength of the stratification at ice onset, which is connected to the strength of the wind forcing. Lakes experience periods of mixing and stratification when cooling below T_{md}, and the depth of the surface mixed layer is often shallower than the full basin depth and thus can both decrease and increase through time [41]. Ultimately, this means that the full depth-averaged temperature of a basin can be above the freezing point at ice onset because either the mixed layer does not span the full depth of the basin, the basin stratifies long enough for the surface to reach the freezing point before mixing again, or more realistically, a combination of the two. If our model allowed the surface mixed layer depth to change continuously through time, then we would expect the basin to freeze when this mixed-layer temperature reached the freezing point, i.e., $\theta_{frz} \equiv -1$. As this is not the case, we have accommodated stratification events and a variable mixed layer depth by allowing $\theta_{frz} \geq -1$.

The accuracy of our analytical prediction for the time of littoral zone ice onset, (33), depends heavily on θ_{frz}. As an example, consider the case where $\theta_{frz} = -0.25$ ($T \approx 3°\text{C}$) in application to BML. In this situation, the littoral zone would experience ice onset during a period of weak exchange with the main basin (see figure 8a), rather than during the assumed quasi-steady period. This would invalidate our assumption that the non-linearity due to the quadratic equation of state was negligible, and our resulting analytical prediction for $t_{f,1}$, (33), would fail. In particular, our prediction for $t_{f,1}$ would be 10 days off, which is a significant error. However, given that littoral zones are by definition shallower than main basins of lakes, if there is enough energy to assume well mixedness of the main basin, it is more likely that the littoral zone will experience ice onset when its depth-averaged temperature is much closer to the freezing temperature. We suspect that this is the case at BML, which explains the under prediction of the ice onset time in the littoral zone.

4.2.4 Role of Friction

Our model has neglected frictional effects, including interfacial friction (at the interface between the two gravity currents), and bottom and side-wall friction in the littoral zone. While the side-wall frictional effects are likely quite small due to the width of the littoral zone in comparison with its depth [13], both the bottom friction and interfacial friction would act to decrease the exchange flow rate in comparison with our inviscid representation [e.g., 14, 24, 46]. For this reason, our model predicts the upper bound on the heat flux due to a purely baroclinic exchange flow.

Under the assumption that any barotropic contribution to exchange between the two basins is negligible, the agreement between our model predictions and the observations would indicate weak frictional effects. The addition of friction would result in earlier ice onset in the littoral zone than observed. This is because a reduction in the exchange flow rate is

equivalent to a reduction in the exchange flow heat flux, and the exchange flow heat flux acts to slow the rate of cooling in the littoral zone. If our model over-predicted the ice onset time in the littoral zone, the neglect of frictional effects might be the obvious culprit. However, our model under-predicts the ice onset time in the littoral zone of BML. While it is possible that frictional effects are opposed by barotropic strengthening of the exchange flow heat flux, assessing this possibility is beyond the scope of the current study.

5 Conclusions

We have derived a simple system of two coupled non-linear ordinary differential equations describing the temperature evolution of the shallow littoral zone and deeper main basin of a fresh-water lake. The model is forced with a constant and uniform surface heat flux from the lake surface to the atmosphere. We assume that water density is a quadratic function of temperature and that each basin remains vertically well mixed, even below the temperature of maximum density, T_{md}. Using both numerical and analytical solutions of our model, we address two open questions: what role does differential cooling around and below T_{md} play in 1) the cooling behaviour of each basin, and 2) the timing of ice onset?

The cooling behaviour of the littoral zone and main basin, respectively, depend upon two heat fluxes in our model: the constant and uniform surface forcing and a time dependent heat flux due to thermally driven exchange between the two basins. When the depth of the littoral zone is small in comparison to that of the main basin (i.e., $\delta \ll 1$), as it is by definition, the cooling rate of the main basin due to the surface forcing alone is much slower than that of the littoral zone. This means that the littoral zone cools more rapidly in relation to the main basin, which can quickly establish a temperature difference between the two basins. When the total volume of water in the littoral zone is small in comparison to that of the main basin (i.e., $\delta \ll 1$ and the surface area ratio $\alpha \ll 1$), the thermal impact of an exchange flow is much greater for the littoral zone than for the main basin.

Taken together, there are two obvious cooling regimes predicted by our model: a weak exchange regime during which differential cooling dominates and temperature differences between the two basins are established, and a quasi-steady state regime during which the warming of the littoral zone due to exchange balances the more rapid cooling due to it being shallower. When the thermal behaviour of the littoral zone has the capacity to be sufficiently dominated by exchange-flow with the main basin (i.e., sufficiently large Φ), the difference in the timing of ice-set between the littoral zone and main basin becomes invariant to initial conditions. Using this invariance to initial conditions, the timing of ice onset in the littoral zone can be solved analytically using (33).

Both our numerical results and analytical predictions reflect the strong dependence of ice onset in the littoral zone upon the magnitude of Φ. Our model accurately predicts the approximate four day lag in ice onset between the littoral zone and main basin of Base Mine Lake (BML), in Alberta, Canada in 2015. This remarkable comparison between simple model output and observations strongly suggests that consideration of an exchange flow with a deeper main basin would allow for better prediction of ice onset in the ecologically sensitive littoral zones of freshwater and brackish lakes.

This work presents a first look in to the role that differential cooling might play in both the behaviour of a cooling lake system around and below T_{md} and consequently in the timing of ice onset in different lake zones. Given the sensitivity and importance of littoral zones [e.g., 43], knowledge on the behaviour of differentially cooling lakes and the impact of lake convection on surface ice onset can have important implications for the ecosystem dynamics of lakes [e.g., 26]. This could be an important consideration in the design of future lake reclamation sites like BML.

Given the nature of this work, there are a number of limitations and remaining open questions which we hope will be pursued further using this model as a basic framework. Firstly, BML is an ideal case study lake for comparison against our simple model. In order to assess whether the model also applies for lakes with less ideal geometries, such as more continuous sloping interfaces between the littoral zone and main basin or a littoral zone which surrounds the entirety of the main basin, comparison against observations made in other lakes is desirable. Other obvious future iterations include the inclusion of interfacial and bottom stress to improve the representation of exchange flow in the model, a temporally varying heat flux at the lake surface to better represent the impact of heating and cooling processes in the system, use of an effective (time dependent) depth ratio to better represent the growth and decay of the surface mixed layer in response to changes in wind forcing, and inclusion of a Coriolis term to better represent the potential impact of Earth's rotation on the exchange flow. Given that the model developed is a coupled system of autonomous non-linear ordinary differential equations, further analysis on the dynamics of the system could be conducted using a phase-plane analysis. Our hope is that this model is used as a basis for further investigation of differentially cooling lake systems that eventually freeze.

Acknowledgements

This research was funded by a Natural Science and Engineering Research Council of Canada (NSERC) Alliance Grant in conjunction with Syncrude Canada Ltd. We would like to thank Dr. Neil Balmforth for his initial guidance with the quasi-steady state solution presented in this manuscript. We would also like to thank Dr. Stephanie Waterman, Dr. Ian Frigaard, and Dr. Marco Tofolon for their feedback on this research.

Data Availability

The temperature and wind speed data taken at Base Mine Lake and shown in this manuscript can be found on Dryad (https://doi.org/10.5061/dryad.s1rn8pkjj). Simple ODE solvers in MATLAB were used to numerically solve the coupled system described in the manuscript.

Author Contributions

KAE: Development of the model and all analysis; writing of manuscript; production of figures; editing of manuscript.
ET: Data collection; data processing; editing of manuscript.
BEL: Editing of manuscript.
MBP: Editing of manuscript.
GAL: Acquired funding for project; editing of manuscript.

A Model Dependence on Problem Geometry

With a better understanding of the impact that Φ and θ_0 have on the solution, we consider the role of basin geometry, represented by δ and α. As discussed in section 3.1, when $\Phi = 0$ for all θ_0 and when $\Phi \ll 1$ for θ_0 close enough to the freezing temperature, the timing of ice onset in the littoral zone, $t_{f,1}$, is inversely proportional to δ and the temperature difference between the two basins at this time, $\Delta\theta(t_{f,1})$, is weakly linearly dependent upon δ. For these small Φ scenarios, the surface forcing I_o is dominant in the cooling of both basins, and thus

the surface area ratio of the two basins, α, has a negligible impact. The question remains whether this δ and α dependence changes when Φ is sufficiently large.

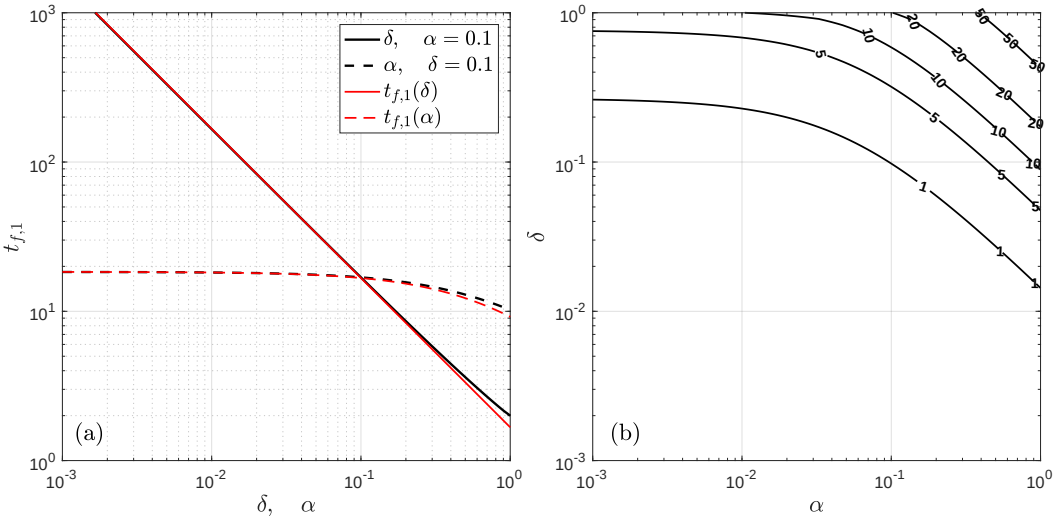

Figure A.1: Impact of lake geometry on the timing of ice onset in the littoral zone ($t_{f,1}$) as predicted by the governing equations (13)–(16) and performance assessment of the analytical prediction (33) for the illustrative heat flux ratio $\Phi = 10$ and initial condition $\theta_0 = 1$. Panel (a) shows both the relation between the depth ratio, δ, and $t_{f,1}$ at fixed surface area ratio, $\alpha = 0.1$, and the relation between α and $t_{f,1}$ at fixed $\delta = 0.1$. The numerical predictions in panel (a) are shown as solid black (varying δ at fixed $\alpha = 0.1$) and dashed black (varying α at fixed $\delta = 0.1$) lines with the corresponding analytical predictions according to (33) shown as solid red (varying δ at fixed $\alpha = 0.1$) and dashed red (varying α at fixed $\delta = 0.1$) lines. Panel (b) provides a comparison between the numerical prediction for $t_{f,1}$ and the analytical prediction given by (33) as a function of both δ and α. As a method of comparison, the percent error between the two predictions was calculated using the numerical solution as the 'observed' value and the analytical prediction as the 'expected' value. The 1%, 5%, 10%, 20%, and 50% error contours are drawn and labelled showing excellent agreement between the numerical solutions and analytical predictions for $\delta \leq 0.1$ and $\alpha \leq 0.1$ at $\Phi = 10$ and $\theta_0 = 1$.

Figure A.1(a) showcases the sensitivity of the timing of ice onset in the littoral zone to both δ and α at fixed $\Phi = 10$ and $\theta_0 = 1$ as solid and dashed black lines, respectively. It is apparent that the inverse dependence of $t_{f,1}$ on δ is retained, even as $\delta \to 1$. However, as $\alpha \to 1$, $t_{f,1}$ becomes increasingly sensitive to α. Regardless, the system is obviously more sensitive to changes in δ than to changes in α. These results are compared against the analytical predictions constructed and discussed in section 3.2, shown as solid and dashed red lines for δ and α, respectively.

B Derivation of Analytical Solution for $\theta_0 = 0$

B.1 Weak Exchange Solution

Because of the initial condition of the system, $\theta_1(0) = \theta_2(0) = \theta_0$, $\phi(0) = 0$, and thus the littoral zone and main basin begin cooling as if they were decoupled. The system (13)–(14)

initially reduces to (18)–(19), which for $\delta \ll 1$, effectively means that the temperature in the main basin, θ_2, is stationary in comparison to the littoral zone. Thus, as the littoral zone rapidly cools, a temperature and density difference between the two basins establishes due to the littoral zone's departure from the initial state. Unlike the case where $\Phi = 0$, however, a non-zero difference in density between the two basins will begin forcing an exchange flow. As the littoral zone cools relative to the main basin, the strength of this exchange flow grows, increasing the effect of the exchange related heat flux on the littoral zone cooling. The ODEs describing this short initial cooling period are thus given by

$$\dot{\theta}_1^W = -1 + \Phi \left| \left(\theta_1^W\right)^2 - \left(\theta_2^W\right)^2 \right|^{1/2} \left(\theta_2^W - \theta_1^W\right) \tag{39}$$

$$\dot{\theta}_2^W = 0, \tag{40}$$

subject to the initial conditions $\theta_1^W(0) = \theta_2^W(0) = 0$. By inspection, the solution to (40) is $\theta_2^W(t) = 0$, which allows us to simplify (39) to

$$\dot{\theta}_1^W = -1 - \Phi \left|\theta_1^W\right| \theta_1^W. \tag{41}$$

In order to solve for θ_1^W, it is useful to define $\theta_1^W = -\Phi^{-1/2} u$ and $t = \Phi^{-1/2} s$, which upon substitution in to (41) gives

$$\frac{\mathrm{d}u}{\mathrm{d}s} = 1 - u^2, \tag{42}$$

which is a separable non-linear ODE whose solution is a hyperbolic tangent. Applying the initial condition, $\theta_1^W(0) = 0$, we obtain the short-time solution for temperature in the littoral zone. The solution during the weak exchange regime is thus given as

$$\theta_1^W(t) = -\Phi^{-1/2} \tanh \Phi^{1/2} t, \tag{43}$$

$$\theta_2^W(t) = 0. \tag{44}$$

The weak exchange solution in the littoral zone is shown as a dotted black line in figure B.1. We can interpret the time and θ_1^W scaling used to solve (41) as the timescale over which $\theta_2 \approx 0$ and the temperature scale that θ_1 approaches over this period of time, respectively. As $\theta_1 \to -\Phi^{-1/2}$, however, $\dot{\theta}_1 \to 0$. This process occurs because a greater density difference between the two basins means a stronger exchange flow, and thus a stronger incoming flux of water from the warmer main basin. This growing flux of warmer water from the main basin acts to decelerate the cooling in the littoral zone, slowing the growth of the exchange between the two basins. Eventually, the littoral zone cooling becomes limited by the cooling in the main basin.

B.2 Quasi-Steady State Solution

During the quasi-steady cooling regime, the littoral zone cooling is balanced by the warming due to exchange with the main basin, and thus $\phi(t) \approx 1$. Expressed differently, during the quasi-steady cooling regime,

$$\left| \left(\theta_1^Q\right)^2 - \left(\theta_2^Q\right)^2 \right|^{1/2} \left(\theta_2^Q - \theta_1^Q\right) = \Phi^{-1} \tag{45}$$

and the rate at which the littoral zone cools will be dictated by the cooling rate in the main basin. Since $\phi(t) \approx 1$, the rate of cooling in the main basin is given by

$$\dot{\theta}_2^Q = -\delta \left(1 + \alpha\right), \tag{46}$$

subject to the initial condition $\theta_2^Q(0) = 0$. We can again solve for θ_2 upon inspection, giving $\theta_2^Q(t) = -\delta\,(1+\alpha)\,t$, which can be substituted in to (45) to solve for θ_1^Q. Before doing so, however, some initial observations are worth making. First of all, since $\Phi > 0$, we require that $\theta_1 < \theta_2$ to satisfy (45). We also know that $\theta_2 < 0$ for all $t > 0$, so $\theta_1 < \theta_2 < 0$. This means that $|\theta_1| > |\theta_2|$, and thus that $\theta_1^2 - \theta_2^2 > 0$. We can therefore neglect the absolute value sign in (45) and rewrite (45) as,

$$\left(\theta_2^Q - \theta_1^Q\right)^{3/2}\left(\theta_1^Q + \theta_2^Q\right)^{1/2} = -\Phi^{-1}. \tag{47}$$

If we further assume that during this cooling period, θ_1 will effectively remain at some set temperature below θ_2, we can substitute $\theta_1^Q = \theta_2^Q - c$, where c is positive. Since our objective is an expression for θ_1^Q, we will only use this substitution to replace $\theta_1^Q + \theta_2^Q = 2\theta_2^Q - c$. Given that prior to this quasi-steady cooling regime, the littoral zone cooled to a value on the order of $\Phi^{-1/2}$ while $\theta_2 \approx 0$, we can immediately replace c with $\Phi^{-1/2}$. We can then rewrite equation (47) as

$$\left(\theta_2^Q - \theta_1^Q\right)^{3/2} = \Phi^{-1}\left(\Phi^{-1/2} - 2\theta_2^Q\right)^{-1/2}. \tag{48}$$

Upon solving for θ_1^Q in (48), we obtain the quasi-steady solutions for temperature in the littoral zone and main basin as,

$$\theta_1^Q(t) = \theta_2^Q(t) - \Phi^{-2/3}\left(\Phi^{-1/2} - 2\theta_2^Q(t)\right)^{-1/3}, \tag{49}$$

$$\theta_2^Q(t) = -\delta\,(1+\alpha)\,t. \tag{50}$$

The quasi-steady solution for the littoral zone is shown as a dot-dashed line in figure 5(b).

B.3 Composite Solution

Since the weak exchange solution for the main basin is zero to leading order (see equation (44)), the quasi-steady state solution for the main basin is the composite solution for the main basin to leading order. In order to construct a composite solution for the littoral zone, we can add the weak-exchange solution, $\theta_1^W(t)$, to the quasi-steady state solution, $\theta_1^Q(t)$, and then ensure that $\theta_1^C(t) \to 0$ in the limit as $t \to 0$. That is, the composite solution for the littoral zone is of the form,

$$\theta_1^C(t) = \theta_1^W(t) + \theta_2^Q(t) + C_1, \tag{51}$$

where $C_1 = \Phi^{-1/2}$ ensures that $\theta_1^C(t) \to 0$ in the limit as $t \to 0$. Upon substitution of (43) and (49) into (51), we obtain the analytical solution (13)–(14) cooled from $\theta_1(0) = \theta_2(0) = 0$, given by

$$\theta_1^C(t) = \theta_2^C(t) - \Phi^{-1/2}\left(\tanh\Phi^{1/2}t - 1\right) - \Phi^{-2/3}\left(\Phi^{-1/2} - 2\theta_2^C(t)\right)^{-1/3}, \tag{52}$$

$$\theta_2^C(t) = -\delta\,(1+\alpha)\,t. \tag{53}$$

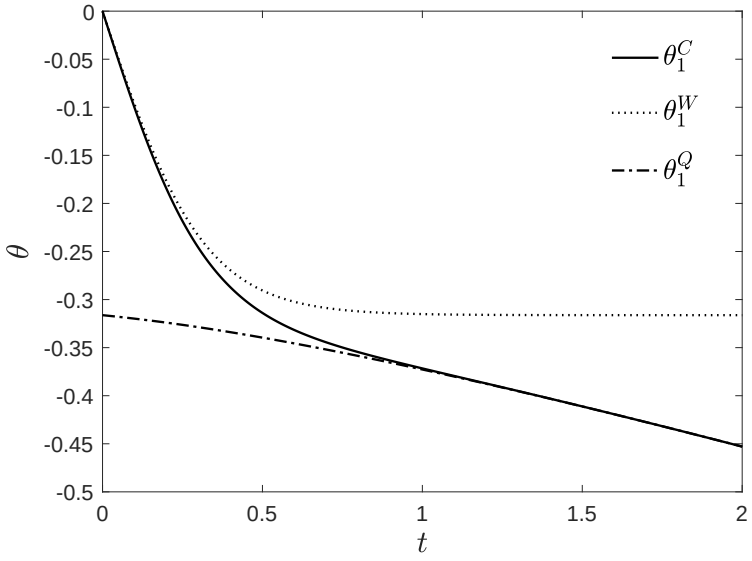

Figure B.1: Analytical composite solution in the littoral zone, θ_1^C (solid black line), and the associated solution during the weak exchange regime, θ_1^W (black dotted line) given by (43), and the solution during the quasi-steady regime, θ_1^Q (dot-dashed black line) given by (49).

References

[1] L. Armi. The hydraulics of two flowing layers with different densities. *Journal of Fluid Mechanics*, 163:27–58, 1986.

[2] M. A. Bilello. Method for predicting river and lake ice formation. *Journal of Applied Meteorology and Climatology*, 3(1):38–44, 1964.

[3] S. Brothers, G. Kazanjian, J. Köhler, U. Scharfenberger, and S. Hilt. Convective mixing and high littoral production established systematic errors in the diel oxygen curves of a shallow, eutrophic lake. *Limnology and Oceanography: Methods*, 15(5):429–435, 2017.

[4] E. C. Carmack. Combined influence of inflow and lake temperatures on spring circulation in a riverine lake. *Journal of Physical Oceanography*, 9(2):422–434, 1979.

[5] S. Chang. *Heat budget for an oil sands pit lake*. PhD thesis, University of British Columbia, 2020. URL https://open.library.ubc.ca/collections/ubctheses/24/items/1.0392976.

[6] C.-T. A. Chen and F. J. Millero. Thermodynamic properties for natural waters covering only the limnological range 1. *Limnology and Oceanography*, 31(3):657–662, 1986.

[7] T. Doda, C. L. Ramón, H. N. Ulloa, A. Wüest, and D. Bouffard. Seasonality of density currents induced by differential cooling. *Hydrology and Earth System Sciences*, 26(2): 331–353, 2022.

[8] T. Doda, C. L. Ramón, H. N. Ulloa, M. S. Brennwald, R. Kipfer, M.-E. Perga, A. Wüest, C. J. Schubert, and D. Bouffard. Lake surface cooling drives littoral-pelagic exchange of dissolved gases. *Science Advances*, 10(4):eadi0617, 2024.

[9] G. H. Elliott. *A laboratory and mathematical study of the "thermal bar"*. PhD thesis, University of British Columbia, 1970. URL https://open.library.ubc.ca/collections/ubctheses/831/items/1.0302462.

[10] K. A. Everard. *Natural Convective Processes*. PhD thesis, University of British Columbia, 2023. URL ??

[11] D. E. Farrow and N. R. McDonald. Coriolis effects and the thermal bar. *Journal of Geophysical Research: Oceans*, 107(C5):1–1, 2002.

[12] I. Fer, U. Lemmin, and S. Thorpe. Winter cascading of cold water in lake geneva. *Journal of Geophysical Research: Oceans*, 107(C6):13–1, 2002.

[13] L. Gu. *Frictional exchange flow through a wide channel with application to the Burlington Ship Canal*. PhD thesis, University of British Columbia, 2001. URL https://open.library.ubc.ca/collections/ubctheses/831/items/1.0063727.

[14] L. Gu and G. A. Lawrence. Analytical solution for maximal frictional two-layer exchange flow. *Journal of Fluid Mechanics*, 543:1–17, 2005.

[15] P. R. Holland and A. Kay. A review of the physics and ecological implications of the thermal bar circulation. *Limnologica*, 33(3):153–162, 2003.

[16] G. Horsch and H. Stefan. Convective circulation in littoral water due to surface cooling. *Limnology and Oceanography*, 33(5):1068–1083, 1988.

[17] D. L. Hurley. *Wind waves and internal waves in Base Mine Lake*. PhD thesis, University of British Columbia, 2017. URL https://open.library.ubc.ca/collections/ubctheses/24/items/1.0351993.

[18] D. M. Imboden and A. Wüest. Mixing mechanisms in lakes. *Physics and chemistry of lakes*, pages 83–138, 1995.

[19] V. Ivanov, G. Shapiro, J. Huthnance, D. Aleynik, and P. Golovin. Cascades of dense water around the world ocean. *Progress in oceanography*, 60(1):47–98, 2004.

[20] G. A. Lawrence. On the hydraulics of boussinesq and non-boussinesq two-layer flows. *Journal of Fluid Mechanics*, 215:457–480, 1990.

[21] G. A. Lawrence. The hydraulics of steady two-layer flow over a fixed obstacle. *Journal of Fluid Mechanics*, 254:605–633, 1993.

[22] C. Lei and J. C. Patterson. Natural convection induced by diurnal heating and cooling in a reservoir with slowly varying topography. *JSME International Journal Series B Fluids and Thermal Engineering*, 49(3):605–615, 2006.

[23] M. Leppäranta. Interpretation of statistics of lake ice time series for climate variability. *Hydrology research*, 45(4-5):673–683, 2014.

[24] S. Li and G. Lawrence. Unsteady two-layer hydraulic exchange flows with friction. *Journal of Fluid Mechanics*, 633:99–114, 2009.

[25] G. E. Liston and D. K. Hall. An energy-balance model of lake-ice evolution. *Journal of Glaciology*, 41(138):373–382, 1995.

[26] S. MacIntyre and J. M. Melack. Vertical and horizontal transport in lakes: linking littoral, benthic, and pelagic habitats. *Journal of the North American Benthological Society*, 14 (4):599–615, 1995.

[27] J. D. McFadden. The interrelationship of lake ice and climate in central canada. Technical report, Wisconsin Univ-Madison Dept of Meteorology, 1965.

[28] S. G. Monismith. Hydrodynamics of coral reefs. *Annual Review of Fluid Mechanics*, 39: 37–55, 2007.

[29] S. G. Monismith, J. Imberger, and M. L. Morison. Convective motions in the sidearm of a small reservoir. *Limnology and Oceanography*, 35(8):1676–1702, 1990.

[30] S. G. Monismith, A. Genin, M. A. Reidenbach, G. Yahel, and J. R. Koseff. Thermally driven exchanges between a coral reef and the adjoining ocean. *Journal of Physical Oceanography*, 36(7):1332–1347, 2006.

[31] A. C. Neumann and D. A. McGill. Circulation of the red sea in early summer. *Deep Sea Research (1953)*, 8(3-4):223–235, 1961.

[32] H. Niemann, C. Richter, H. M. Jonkers, and M. I. Badran. Red sea gravity currents cascade near-reef phytoplankton to the twilight zone. *Marine Ecology Progress Series*, 269:91–99, 2004.

[33] J. Olsthoorn, E. W. Tedford, and G. A. Lawrence. The cooling box problem: convection with a quadratic equation of state. *Journal of Fluid Mechanics*, 918:A6, 2021.

[34] C. L. Ramón, H. N. Ulloa, T. Doda, and D. Bouffard. Flushing the lake littoral region: the interaction of differential cooling and mild winds. *Water Resources Research*, 58(3): e2021WR030943, 2022.

[35] W. F. Rannie. Breakup and freezeup of the red river at winnipeg, manitoba canada in the 19th century and some climatic implications. *Climatic Change*, 5:283–296, 1983.

[36] Y. R. Rao and D. J. Schwab. Transport and mixing between the coastal and offshore waters in the great lakes: a review. *Journal of Great Lakes Research*, 33(1):202–218, 2007.

[37] L. F. Shampine and M. W. Reichelt. The matlab ode suite. *SIAM journal on scientific computing*, 18(1):1–22, 1997.

[38] J. J. Sturman, C. E. Oldham, and G. N. Ivey. Steady convective exchange flows down slopes. *Aquatic Sciences*, 61(3):260–278, 1999.

[39] T. Sugimoto and J. A. Whitehead. Laboratory models of bay-type continental shelves in the winter. *J. Phys. Oceanogr*, 13(10):1819–1828, 1983.

[40] E. Tedford, G. Halferdahl, R. Pieters, and G. A. Lawrence. Temporal variations in turbidity in an oil sands pit lake. *Environmental Fluid Mechanics.*, 19:457–473, 2019.

[41] M. Toffolon, L. Cortese, and D. Bouffard. Self v1.0: a minimal physical model for predicting time of freeze-up in lakes. *Geoscientific Model Development*, 14(12):7527–7543, 2021. doi: 10.5194/gmd-14-7527-2021.

[42] H. N. Ulloa, C. L. Ramón, T. Doda, A. Wüest, and D. Bouffard. Development of overturning circulation in sloping waterbodies due to surface cooling. *Journal of Fluid Mechanics*, 930, 2022.

[43] R. G. Wetzel and G. E. Likens. *The Littoral Zone*, pages 313–324. Springer New York, New York, NY, 2000. ISBN 978-1-4757-3250-4.

[44] J. Whitehead, Jr. Laboratory models of circulation in shallow seas. *Philosophical Transactions of the Royal Society of London. Series A, Mathematical and Physical Sciences*, 302(1472):583–595, 1981.

[45] J. A. Whitehead. A laboratory model of cooling over the continental shelf. *Journal of Physical Oceanography*, 23:2412 – 2427, 1993.

[46] L. J. Zaremba, G. Lawrence, and R. Pieters. Frictional two-layer exchange flow. *Journal of Fluid Mechanics*, 474:339–354, 2003.

[47] K. Zhao. *Ebullition from lake sediments*. PhD thesis, University of British Columbia, 2023. URL https://open.library.ubc.ca/collections/ubctheses/24/items/1.0424309.